Journal of Molecular Structure 1200 (2020) 127089

Contents lists available at ScienceDirect

Journal of Molecular Structure

journal homepage: http://www.elsevier.com/locate/molstruc

Theoretical and experimental study of torsional potentials, molecular structure (monomer and dimer), vibrational analysis and molecular characteristics of some dimethyl bipyridines

L. Ravindranath [a], B. Venkatram Reddy [b, *]

[a] Department of Physics, New Science Degree and P.G. College, Warangal, 506001, Telangana, India
[b] Department of Physics, Kakatiya University, Warangal, 506009, Telangana, India

ARTICLE INFO

Article history:
Received 30 July 2019
Received in revised form
14 September 2019
Accepted 17 September 2019
Available online 20 September 2019

Keywords:
Dimethyl-bipyridines
Vibrational spectra
NMR spectra
UV–Vis spectra
Inter-molecular hydrogen bond
DFT

ABSTRACT

This study deals with the determination of torsional potentials, molecular geometry in monomer and dimer form and vibrational assignments of 4,4′-dimethyl-2,2′-bipyridine (4DB); 5,5′-dimethyl-2,2′-bipyridine (5DB); and 6,6′-dimethyl-2,2′-bipyridine (6DB) using quantum chemical calculations carried out by density functional theory (DFT) employing B3LYP functional in conjunction with 6−311++G(d,p) basis set. Existence of inter-molecular hydrogen bonds was predicted. Fourier Transform infrared (FTIR) and Fourier Transform Raman (FT-Raman) spectra were recorded and vibrational analysis of the molecules was made using potential energy distribution (PED) and eigen vectors obtained in the computations. Observed and calculated frequencies agreed with an rms error 9.20, 8.21, and 8.33 cm^{-1} for 4DB, 5DB, and 6DB, respectively. ^{1}H and ^{13}C NMR spectra were simulated using time-dependent DFT (TD-DFT); compared with the recorded experimental spectra of the samples in Chloroform-d ($CDCl_3$) solvent and observed that the chemical shifts agree well with their theoretical counterparts. Electronic transitions were analyzed using experimental and simulated UV–Vis spectra of the three molecules. Molecular characteristics like HOMO-LUMO; thermodynamic parameters; and molecular electrostatic surface potential (MESP) quantified with natural charges obtained by NBO analysis are also investigated.

1. Introduction

Bipyridine and its derivatives have been widely used since its first design as ligand in the fields of inorganic, organometallic, supra-molecular and macromolecular chemistry for the complexation of metal centres and as chelate systems in coordination chemistry [1,2]. They acquire exceptional electronic structure that occurs due to π-bond conjugated system in pyridine rings and two dynamic nitrogen atoms. They exhibit competent binding for many metals due to the unique chelating effect and the ability of acceptance [3]. Hence, bipyridines along with their metal complexes have become materials of massive importance in broad range of applications such as herbicides [4,5], biologically active new materials [6]; and organic LEDs, NLO materials, luminescent sensors and artificial synthesis [7–9].

Though, the significance of bipyridines and their derivatives is established, but the quantum chemical computations were not carried out to investigate the optimized molecular geometry, molecular characteristics and vibrational properties of many bipyridine derivatives. Taking this as inspiration, we have demonstrated such studies for 2,2′-bipyridine (2BPE); 4,4′-bipyridine (4BPE); and 2,4′-bipyridine [10] and bipyridine-dicarboxylic acids [11] in our earlier work. As a continuation to this type of work, we have now undertaken the investigation on 4,4′-dimethyl-2,2′-bipyridine (4DB); 5,5′-dimethyl-2,2′-bipyridine (5DB); and 6,6′-dimethyl-2,2′-bipyridine (6DB) for the determination of structure, vibrational and molecular properties using vibrational spectra and Scaled Quantum Mechanical (SQM) computations employing density functional theory (DFT).

Silva et al. [12] presented the optimized molecular geometry, calculated total energies and zero-point vibrational energy; and standard molar enthalpies of formation for 4,4′-dimethyl-2,2′-bipyridine using DFT employing different basis sets. Solid state structure and crystallographic data were reported for 4,4′-dimethyl-2,2′-bipyridine; 5,5′-dimethyl-2,2′-bipyridine; and 6,6′-dimethyl-2,2′-bipyridine, respectively by Zhong [13]; Khoshtarkib

* Corresponding author.
E-mail address: bvreddy67@yahoo.com (B.V. Reddy).

https://doi.org/10.1016/j.molstruc.2019.127089
0022-2860/

et al. [14] and Sengul et al. [15]. Solvent effect on molecular geometry and electronic spectra of 6,6′-dimethyl-2,2′-bipyridine was demonstrated based on quantum mechanical computations using a solvent dielectric continuum model and time-dependent DFT by Blanchet-Boiteux et al. [16]. Bator et al. [17] investigated the structure, vibrations and, phase transitions and methyl group tunneling of 4,4′-dimethyl-2,2′-bipyridine; 5,5′-dimethyl-2,2′-bipyridine; and 6,6′-dimethyl-2,2′-bipyridine complexes with chloranilic acid. The stacking behavior of 4,4′-dimethyl-2,2′-bipyridine with quinoxalineplatinum (II) complex was studied by X-ray crystallography and pulsed gradient spin-echo NMR and its cytotoxicity was determined to facilitate structure-activity relationships by Benjamin et al. [18]. Seyfi et al. [19] investigated the molecular structure, bonding characteristics in 6,6′-dimethyl-2,2′-bipyridine and HgI_2 complex using UV–Visible and electronic spectra; and frontier molecular orbital description predicted by time-dependent DFT calculations. 1D, 2D supramolecular structures using elemental analysis, single-crystal and powder XRD analyses; heat capacities; and thermodynamic function values of lanthanide complex of 5,5′-dimethyl-2,2′-bipyridine were determined by Y. Y. Li et al. [20].

Thus, the review of literature signifies that the experimental and theoretical treatment was mainly focused on complexation of different transition metals with various dimethyl-bipyridines. Molecular structure, total energies, crystal structure parameters and thermodynamic parameters of the compounds under investigation were only reported in the literature. However, these compounds were not paid attention on other aspects such as the computation of torsional potentials, which is an important parameter in bipyridines and their derivatives. Hydrogen bonding due to intra-molecular and inter-molecular interactions in dimeric structure; frontier molecular orbital energies; study of electronic transitions from UV–Vis spectra; molecular electrostatic surface potential (MESP) quantified with NBO atomic charges, thermodynamic parameters and rotational constants of these compounds were not investigated earlier. Hence, a systematic spectroscopic (IR,

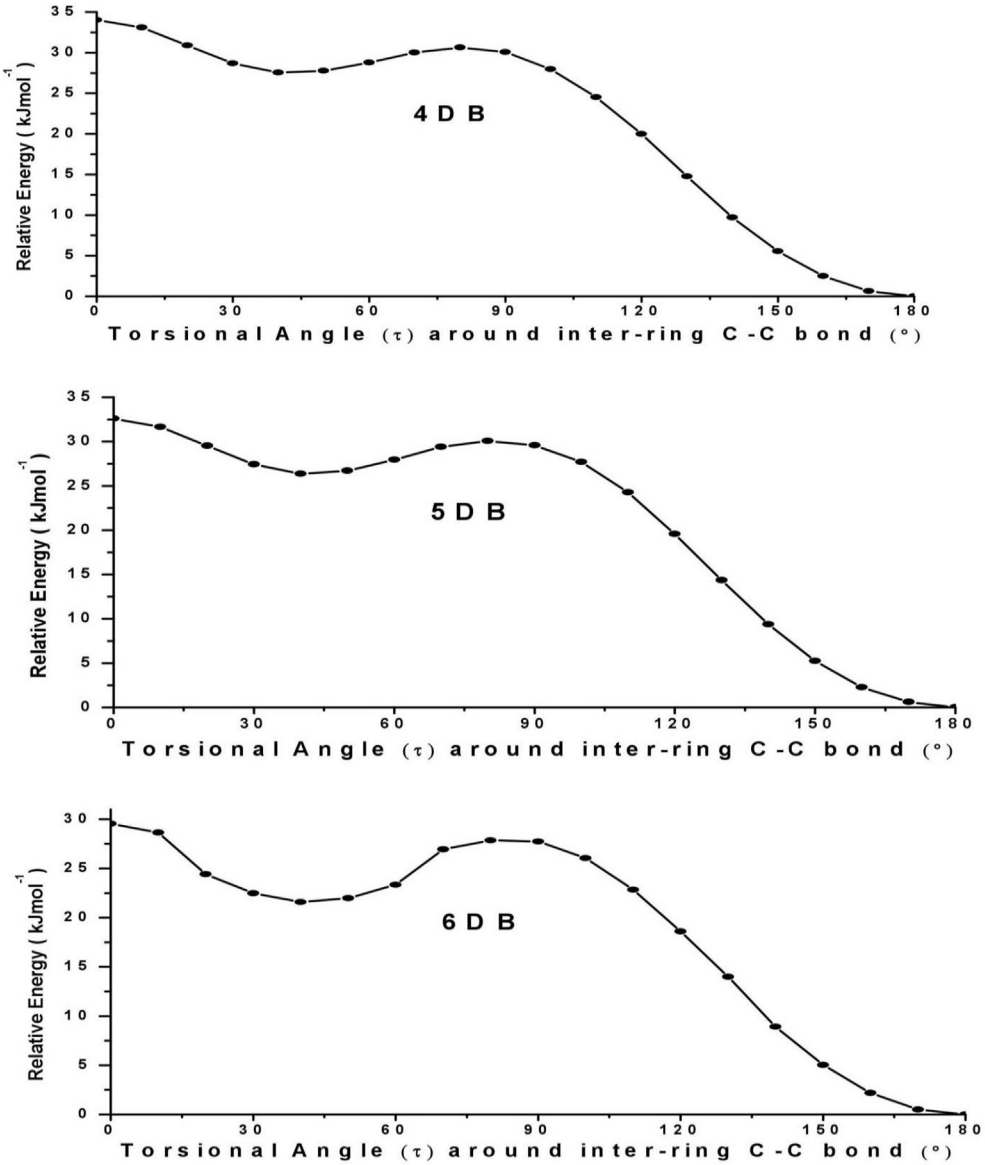

Fig. 1. Relative torsional potential energy as a function of rotation angle (C6–C1–C7–C12) around C–C inter-ring bond for 4BP, 5BP and 6BP using DFT/B3LYP/6-311++G(d,p) formalism.

Raman, ^{1}H NMR and ^{13}C NMR) investigation of 4DB, 5DB and 6DB employing density functional theory (DFT) is undertaken to study the various molecular characteristics and the results are reported in this manuscript.

2. Recording of spectra

The chosen compounds 4DB, 5DB and 6DB, which are solids at room temperature, were procured with high purity from TCI chemical company, Japan and recorded their spectra without further purification. The FTIR spectra of these samples were recorded in the spectral range 4000-450 cm^{-1} by diluting them in KBr pellet, using Nicolet-740 single beam FT-IR spectrometer, equipped with deuterated triglycine sulphate (DTGS) detector. The FT-Raman spectra of the samples were measured, in the 4000-50 cm^{-1} Stokes region, using BRUKER RFS-27 spectrometer

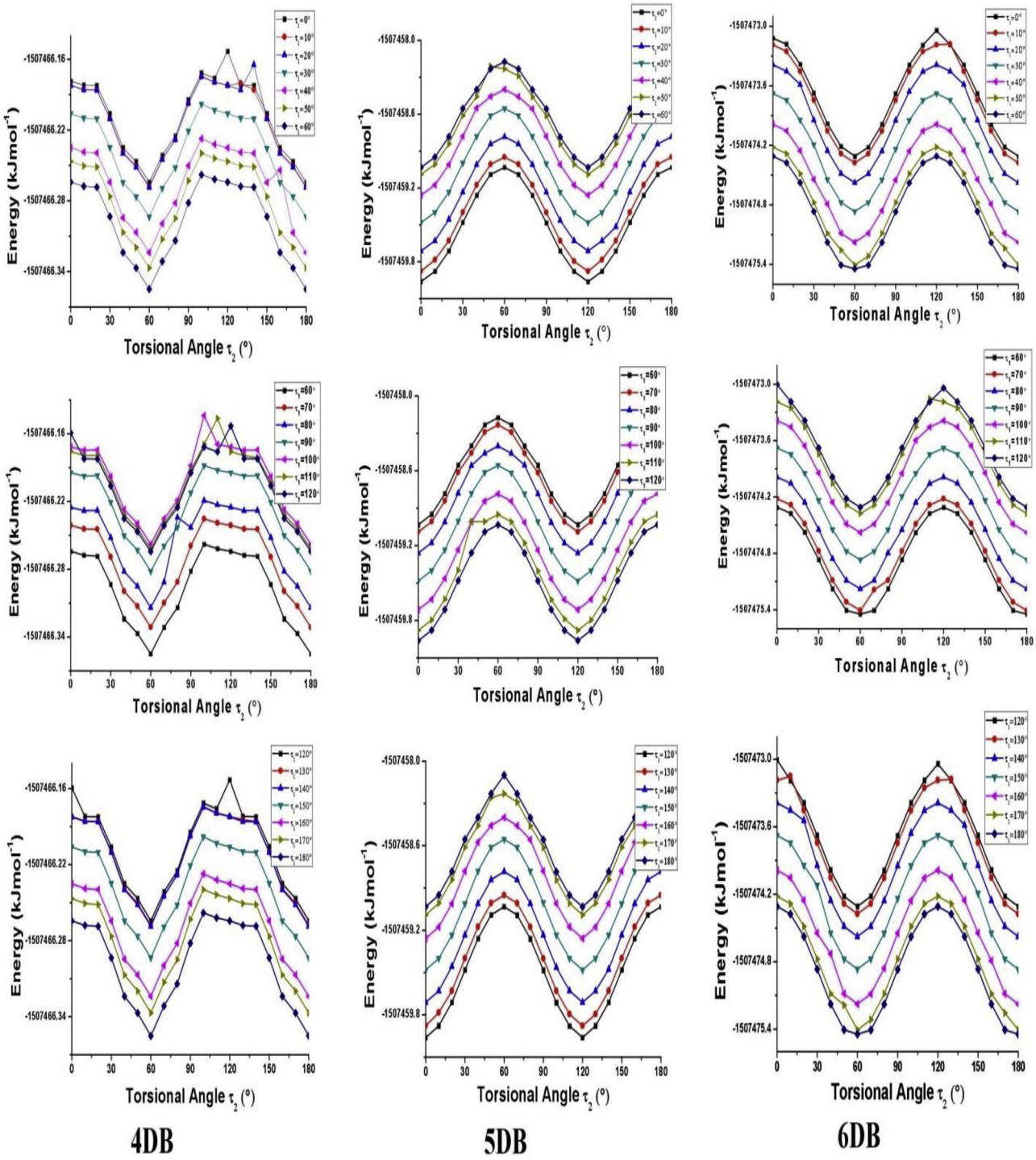

Fig. 2. Absolute energies (kJ mol^{-1}) for different conformers corresponding to various torsion angles (°) around pyridine rings and methyl groups C-C_α bond (τ_1 and τ_2) for 4DB, 5DB and 6DB when the torsion angle C6—C1—C7—C12 around inter-ring C—C bond (τ) is 180°.

employing the exciting radiation at 1064 nm being provided by Nd-YAG laser operating at 200 mw power. ^{1}H and ^{13}C NMR spectra were recorded at room temperature by Bruker Avance HD 500 MHz NMR instrument using Deuterated Chloroform ($CDCl_3$) as solvent. The UV–Visible spectra of the compounds in a solution of DMSO-d_6 using 1 cm quartz cell were recorded in the range 200–400 nm on PerkinElmer UV–Visible LAMBDA-25 double beam spectrophotometer.

3. Computational details

The desired computations were carried out using DFT [21] with three parameter hybrid exchange functional proposed by Beck B3 [22] along with correlational functional of Lee-Yang-Parr [23] employing the split valence triple basis set i.e., 6-311++G(d,p).

In order to get significant results, the most stable conformer that is very close to the final one is to be determined first. But, this becomes tedious task in the case of complex molecules of present type in this investigation. Because, there are three C–C bonds in each of the three molecules, around which rotation is allowed. They are, one C–C bond which acts as interlink between the two pyridine rings and two C–C bonds (C-C_α bonds) between pyridine ring and two methyl groups. Computations cannot be commenced by presumption of the dihedral angles which may be lead to give improbable results. Thus, systematic and meticulous theoretical computations were carried out to calculate the torsion angles for each of the three molecules, which can be used as starting values for subsequent calculations. Keeping this fact in view, the torsional potential energy was calculated as a function of angle of rotation around the C–C pyridine inter-link bond in intervals of 10° between 0° and 180° using Gaussian09W software package implemented on Pentium-V (3.2 GHz) workstation. The results are depicted graphically in Fig. 1. It can be observed that the minimum energies take place at the torsional angle (τ) at 180° in 4DB, 5DB and 6DB. Subsequently, this torsional angle (τ) around C–C bond between inter-pyridine rings is fixed at 180°, the dihedral angle (τ_1) around C-C_α bond between first pyridine ring and one methyl group is varied in steps of 10° between 0° and 180° by changing another dihedral angle (τ_2) around the C-C_α bond between the second pyridine ring and other methyl group in steps of 10° between 0° and 180°. The minimum energies are attained as -1507.466×10^3 and -1507.475×10^3 kJmol^{-1} for the dihedral angles τ_1 and τ_2 at 60° and 180^{0}for 4DB and 6DB, respectively. Similarly, the energy minimum is obtained as -507.459×10^3 kJmol^{-1} for the dihedral angles τ_1 and τ_2, respectively at 120° and 0° for 5DB, as shown in Fig. 2. In this process, 19 data sets, each consisting of 19 data points for a given molecule is resulted. In each data set, the minimum energy conformer and the corresponding angle of rotation τ_1 around the C-C_α bond for each of the three molecules are identified and the values are depicted in Table 1. Likewise, 19 such rotamers were resulted for each molecule. Later, plots were drawn, for each of the three molecules, between the energy of rotamer with respect to the energy of rotamer of lowest energy and angle of rotation τ_2 around the C-C_α bond, from which the dihedral angle τ_1 around the C-C_α bond corresponding to the most stable rotamer is obtained. This can be seen from Table 1 and Figs. 2 and 3. Thus, three torsion angles, one for the C–C inter-ring bond and the other two for C-C_α bonds are computed, for each of the three molecules, which can be used as initial value for subsequent computations. Permitting all structural parameters to settle down simultaneously, the lowest energy conformer in each case, as acquired above, was subjected to meticulous geometry optimization. As a result, equilibrium molecular structure is obtained in monomer form for the three molecules 4DB, 5DB and 6DB with minimum energy -1507.483×10^3, -1507.479×10^3 and -1507.492×10^3 kJ mol^{-1}, respectively. This process gave up the molecular structure with C_1 symmetry for the three molecules. Nonexistence of imaginary or negative frequencies in the computational process demonstrated the reliability of the result for the optimized structure.

Harmonic vibrational frequencies, vibrational cartesian force constants, and the dipole moment and its derivatives were determined for the three molecules in equilibrium geometry with C_1 symmetry. The equilibrium geometry and associated force constants were used as initial data in the remaining computations.

Table 1
Absolute and relative energies (kJ mol^{-1}) for different conformers corresponding to various torsion angles (°) around pyridine rings and methyl groups C-C_α bond (τ_1 and τ_2) for 4DB, 5DB and 6DB when the torsion angle C6–C1–C7–C12 around inter-ring C–C bond (τ) is 180°.

τ_2[a]	Energy of the conformers in kJmol^{-1}						τ_1[b]		
	4DB		5DB		6DB		4DB	5DB	6DB
	Absolute	Relative[c]	Absolute	Relative	Absolute	Relative			
0	−1507466.264	0.091	**−1507459.961**	**0.000**	−1507474.309	1.136	60 &180	**0** & 120	60 &180
10	−1507466.268	0.087	−1507459.878	0.083	−1507474.376	1.069	60 &180	0 & 120	60 &180
20	−1507466.269	0.086	−1507459.712	0.249	−1507474.576	0.869	60 &180	0 & 120	60 &180
30	−1507466.294	0.061	−1507459.481	0.480	−1507474.867	0.578	60 &180	0 & 120	60 &180
40	−1507466.324	0.031	−1507459.258	0.703	−1507475.177	0.268	60 &180	0 & 120	60 &180
50	−1507466.337	0.018	−1507459.09	0.871	−1507475.407	0.038	60 &180	0 & 120	60 &180
60	**−1507466.355**	**0.000**	−1507459.033	0.928	**−1507475.445**	**0.000**	**60** &180	0 & 120	**60**&180
70	−1507466.331	0.024	−1507459.091	0.870	−1507475.408	0.037	60 &180	0 & 120	60 &180
80	−1507466.314	0.041	−1507459.26	0.701	−1507475.178	0.267	60 &180	0 & 120	60 &180
90	−1507466.282	0.073	−1507459.484	0.477	−1507474.869	0.576	60 &180	0 & 120	60 &180
100	−1507466.258	0.097	−1507459.714	0.247	−1507474.578	0.867	60 &180	0 & 120	60 &180
110	−1507466.262	0.093	−1507459.879	0.082	−1507474.377	1.068	60 &180	0 & 120	60 &180
120	−1507466.264	0.091	**−1507459.961**	**0.000**	−1507474.309	1.136	60 &180	0 &**120**	60 &180
130	−1507466.268	0.087	−1507459.878	0.083	−1507474.376	1.069	60 &180	0 & 120	60 &180
140	−1507466.269	0.086	−1507459.712	0.249	−1507474.576	0.869	60 &180	0 & 120	60 &180
150	−1507466.294	0.061	−1507459.481	0.480	−1507474.867	0.578	60 &180	0 & 120	60 &180
160	−1507466.324	0.031	−1507459.258	0.703	−1507475.177	0.268	60 &180	0 & 120	60 &180
170	−1507466.337	0.018	−1507459.09	0.871	−1507475.407	0.038	60 &180	0 & 120	60 &180
180	**−1507466.355**	**0.000**	−1507459.033	0.928	**−1507475.445**	**0.000**	60 &**180**	0 & 120	60 &**180**

[a] Dihedral angle around C-C_α bond.
[b] Dihedral angle around C-C_α bond.
[c] Difference of lowest energy of the given conformer and the energy of the corresponding conformer.

Following the suggestions of Fogarasi et al. [24], the force constants obtained in the computations were transformed into a non-redundant set of 72 natural internal coordinates achieved from 103 redundant internal coordinates using MOLVIB 7.0 Program [25,26]. The force constants were scaled based on the method proposed by Fogarasi and Pulay [27] and Arenas et al. [28] with least-square refinement process so as to make good frequency fit between observed and calculated values. The normal modes of vibrations are exemplified by fundamental frequencies and corresponding eigenvectors, potential energy distribution (PED), relative infrared absorption intensities [29] and relative Raman Scattering intensities [30,31]. IR and Raman spectra of 4DB, 5DB, and 6DB were simulated employing a pure Lorenzian band shape with full width at half maximum (FWHM) of 10 cm^{-1}. The simulated spectra were compared with corresponding experimental spectra. Using the equilibrium geometry with lowest energy of each of the three molecules, the dimeric structure of 4DB, 5DB and 6DB were subjected to geometry optimization at the same level of theory as the corresponding monomer so as to understand the nature of hydrogen bonding in them.

Chemical shifts in ^{1}H and ^{13}C NMR spectra were computed employing gauge-independent or gauge-including atomic orbital (GIAO) approach [32] with DFT/B3LYP/6-311++G(d,p) method, with reference to $CDCl_3$. Solvent effects were considered by the Polarizable Continuum Model (PCM) using the integral equation formalism (IEF-PCM) variant [33] implemented in Gaussian 09 software package. Resulting simulated NMR spectra of the three molecules were compared with corresponding experimental

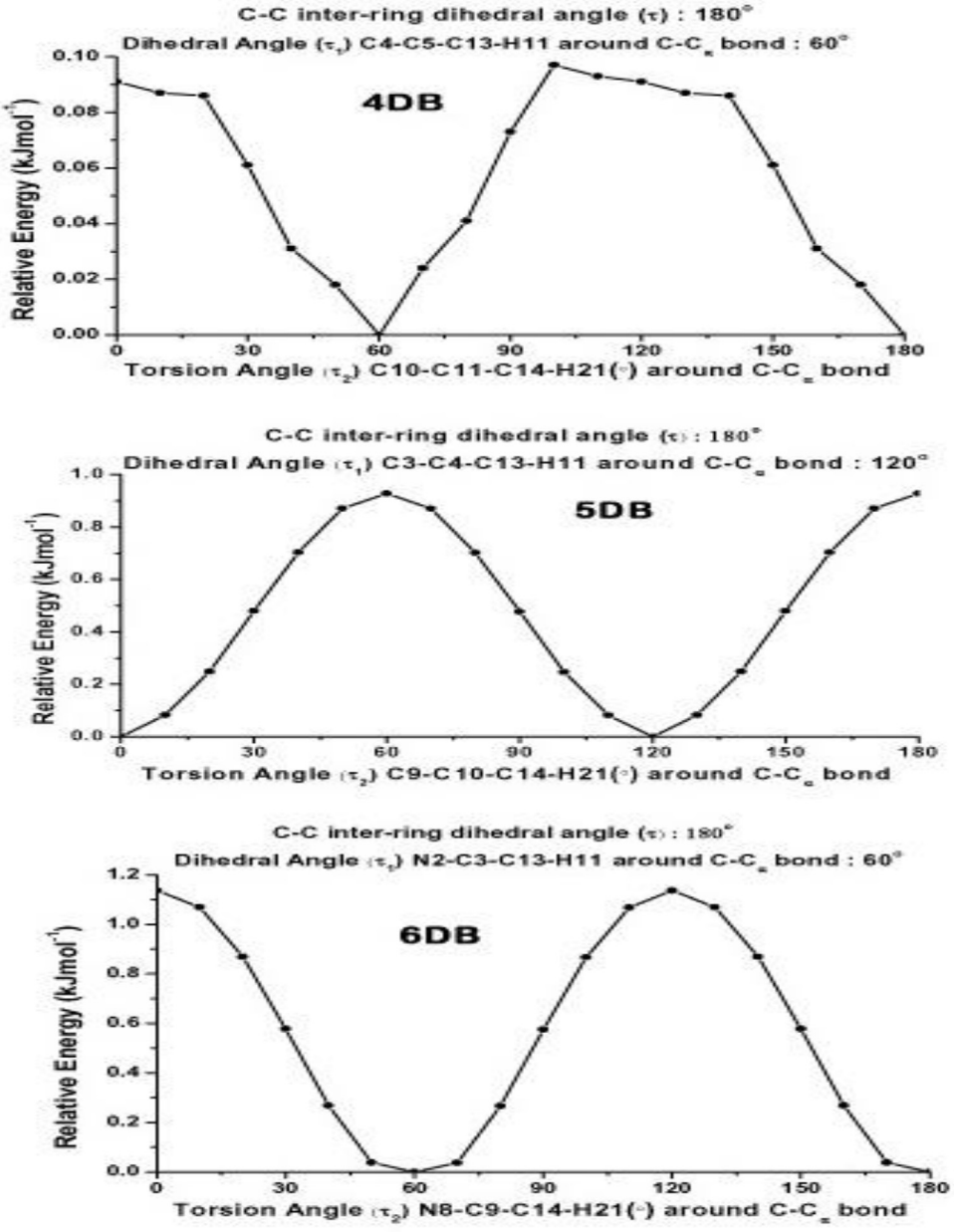

Fig. 3. Relative torsional potential energy as a function of rotation angle around C-C_α bond (τ_2) for 4DB, 5DB and 6DB using DFT/B3LYP/6-311++G (d,p) formalism when the torsion angle around inter-ring C—C bond (τ) is 180° and Dihedral angle (τ_1) at 60° for 4DB and 6DB and 120° for 5DB.

spectra.

The electronic absorption spectrum relating various electronic transitions of 4DB, 5DB and 6DB were computed with Time-Dependent Density Functional Theory (TD-DFT), using B3LYP/6-311++G (d,p) method. Resulting spectrum was compared with corresponding experimental UV−Visible spectrum.

Molecular electronic properties such as ionization potential (I), electron affinity (A), global hardness (η), chemical potential (μ), global electrophilicity power (ω) of 4DB, 5DB and 6DB were obtained from frontier molecular orbital energies comprising of HOMO (Highest Occupied Molecular Orbital) and LUMO (Lowest Unoccupied Molecular Orbital) using the following expressions [34–37].

$$I = -E_{HOMO};\ A = -E_{LUMO};\ \eta = (-EHOMO + ELUMO)/2;$$

$$\mu = (E_{HOMO} + E_{LUMO})/2;\ and\ \omega = \mu^2/2\eta$$

where, E_{HOMO} and E_{LUMO} are HOMO and LUMO orbital energies, respectively.

Other molecular characteristics viz, thermodynamic parameters and rotational constants were determined and the molecular electrostatic surface potential (MESP) is acquired by mapping of molecular electrostatic potential (MEP).

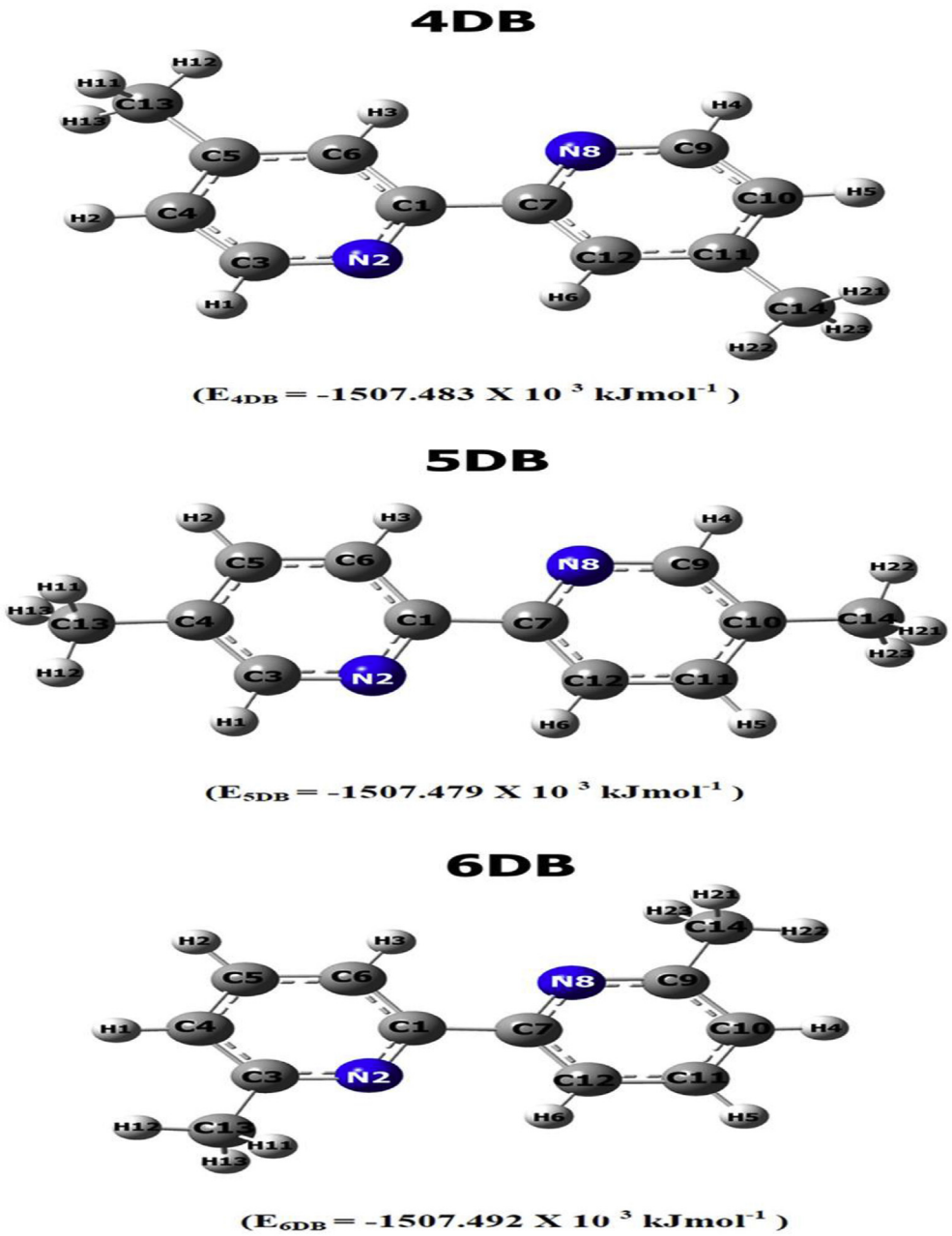

Fig. 4. Optimized molecular structure of 4DB, 5DB and 6DB monomers along with numbering of atoms and minimum energy.

4. Results and discussion

4.1. Molecular geometry in the ground state

The data desired for creating initial values of three torsional angles, one around C—C bond (τ) and the other two angles (τ_1, τ_2) around two C-C_α bonds, those determine the lowest energy conformer obtained as discussed in section 3, are shown in Table 1 and graphically presented in Fig. 3 for the three molecules. This data is represented graphically for rotation around C—C inter-ring bond and two C-C_α bonds in Figs. 1 and 2, respectively, for the three molecules. From Table 1; and Figs. 1—3, it can be observed that the set of three torsional angles (τ, τ_1, τ_2) are determined as (180°, 60°, 60°), (180°, 120°, 120°) and (180°, 60°, 60°) and after refinement in the optimization process, they are obtained as (180.00°, 59.48°, 58.60°), (180.00°, 120.22°, 120.22°) and (180.00°, 59.07°, 59.04°) respectively for 4DB, 5DB and 6DB.

Molecular geometry obtained by solving self-consistent field equations iteratively is depicted in Fig. 4 along with the minimum energy for the three molecules. Optimized geometry for the dimers of 4DB, 5DB and 6DB, obtained from the corresponding monomer structure, is shown in Fig. 5 along with numbering of atoms,

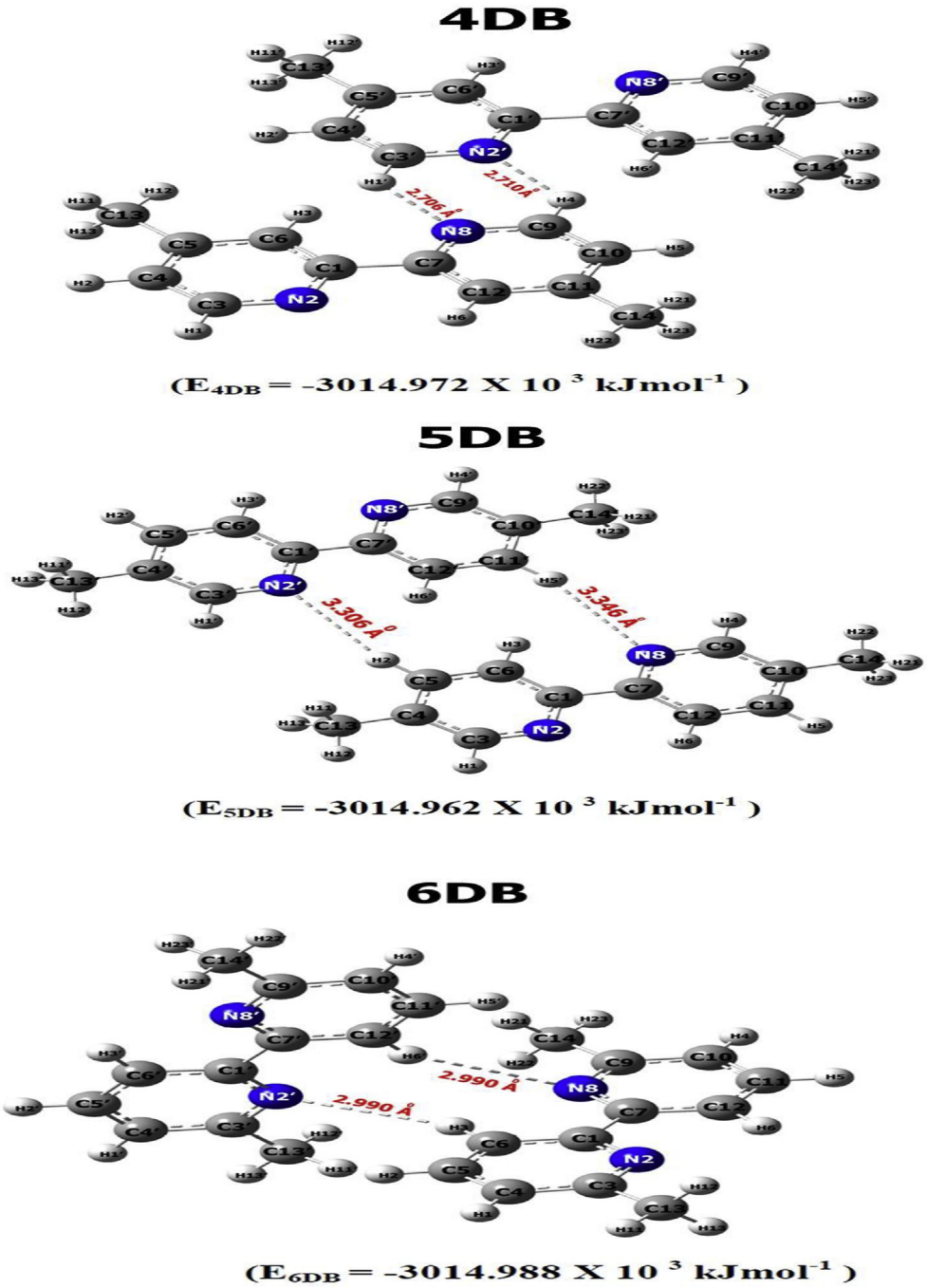

Fig. 5. Optimized molecular structure of 4DB, 5DB and 6DB dimers along with numbering of atoms, inter-molecular hydrogen bonding and minimum energy.

Table 2
Experimental and DFT/B3LYP/6-311++G(d,p) optimized geometric parameters of 4DB,5DB, 6DB and their dimer.

Geometric parameter	4DB			5DB			6DB		
	Calculated Value		Expt. Value[a]	Calculated Value		Expt. Value[b]	Calculated Value		Expt. Value[c]
	Monomer	Dimer		Monomer	Dimer		Monomer	Dimer	
Bond lengths (in Å)									
C1–N2	1.341	1.342	1.342	1.340	1.341	1.334	1.341	1.341	1.353
N2–C3	1.334	1.333	1.339	1.333	1.333	1.340	1.338	1.338	1.338
C3–C4	1.390	1.391	1.383	1.397	1.398	1.389	1.399	1.399	1.390
C4–C5	1.399	1.398	1.386	1.399	1.399	1.371	1.392	1.392	1.383
C5–C6	1.392	1.393	1.390	1.386	1.387	1.384	1.388	1.388	1.377
C6–C1	1.401	1.400	1.386	1.401	1.401	1.393	1.400	1.400	1.386
C1–C7	1.492	1.492	1.479	1.489	1.489	1.491	1.493	1.493	1.485
C7–N8	1.341	1.342	1.348	1.340	1.341	1.334	1.341	1.341	1.353
N8–C9	1.334	1.336	1.334	1.333	1.334	1.340	1.338	1.339	1.338
C9–C10	1.390	1.391	1.371	1.397	1.397	1.389	1.399	1.399	1.390
C10–C11	1.399	1.399	1.391	1.399	1.399	1.371	1.392	1.392	1.383
C11–C12	1.392	1.393	1.393	1.386	1.386	1.384	1.388	1.388	1.377
C12–C7	1.401	1.400	1.383	1.402	1.402	1.393	1.400	1.401	1.386
C5–C13	1.507	1.507	1.502	–	–	–	–	–	–
C11–C14	1.507	1.507	1.499	–	–	–	–	–	–
C4–C13	–	–	–	1.506	1.506	1.511	–	–	–
C10–C14	–	–	–	1.506	1.506	1.511	–	–	–
C3–C13	–	–	–	–	–	–	1.507	1.507	1.503
C9–C14	–	–	–	–	–	–	1.507	1.507	1.503
C3–H1	1.087	1.087	0.930	1.088	1.088	0.930	–	–	–
C4–H1	–	–	–	–	–	–	1.084	1.084	*
C4–H2	1.085	1.085	0.930	–	–	–	–	–	–
C5–H2	–	–	–	1.086	1.086	0.930	1.085	1.084	*
C6–H3	1.082	1.082	0.930	1.081	1.080	0.930	1.081	1.081	*
C9–H4	1.087	1.087	0.930	1.088	1.088	0.930	–	–	–
C10–H4	–	–	–	–	–	–	1.084	1.084	*
C10–H5	1.085	1.085	0.930	–	–	–	–	–	–
C11–H5	–	–	–	1.086	1.086	0.930	1.085	1.085	*
C12–H6	1.082	1.082	0.930	1.081	1.081	0.930	1.081	1.081	*
C13–H11	1.094	1.093	0.960	1.094	1.094	0.960	1.093	1.093	*
C13–H12	1.091	1.092	0.960	1.092	1.092	0.960	1.091	1.093	*
C13–H13	1.094	1.095	0.960	1.094	1.092	0.960	1.093	1.092	*
C14–H21	1.094	1.093	0.960	1.094	1.094	0.960	1.093	1.093	*
C14–H22	1.091	1.091	0.960	1.092	1.092	0.960	1.091	1.093	*
C14–H23	1.094	1.095	0.960	1.094	1.094	0.960	1.093	1.091	*
Bond angle (in °)									
C1–N2–C3	117.67	117.74	116.7	118.51	118.41	117.36	119.44	119.45	118.37
N2–C3–C4	123.77	123.78	123.2	124.52	124.56	125.26	121.75	121.75	122.28
C3–C4–C5	119.07	119.04	120.1	116.32	116.43	116.29	118.88	118.86	119.06
C4–C5–C6	117.18	117.19	116.9	120.03	119.76	119.99	119.31	119.38	118.94
C5–C6–C1	119.90	119.96	119.5	118.94	119.19	119.51	118.31	118.22	*
C6–C1–N2	122.40	122.28	123.5	121.68	121.65	121.57	122.30	122.33	*
N2–C1–C7	117.00	117.05	114.9	117.31	117.27	116.75	116.93	116.72	116.50
C6–C1–C7	120.60	120.66	121.6	121.01	121.08	121.68	120.77	120.95	*
C7–N8–C9	117.69	117.84	119.9	118.50	118.43	117.36	119.45	119.44	118.37
N8–C9–C10	123.77	123.47	123.4	124.52	124.62	125.26	121.75	121.78	122.28
C9–C10–C11	119.06	119.25	119.7	116.32	116.28	116.29	118.88	118.86	119.06
C10–C11–C12	117.19	117.20	118.4	120.03	120.01	119.99	119.31	119.30	118.94
C11–C12–C7	119.92	119.87	120.7	118.94	119.04	119.51	118.31	118.38	*
C12–C7–N8	122.36	122.36	*	121.69	121.61	121.57	122.30	122.22	*
N8–C7–C1	117.11	117.14	116.5	117.28	117.52	116.75	116.92	117.09	*
C12–C7–C1	120.52	120.50	*	121.03	120.87	121.68	120.77	120.67	*
N2–C3–C13	–	–	–	–	–	–	116.50	116.51	116.12
C4–C3–C13	–	–	–	–	–	–	121.74	121.73	*
C3–C4–C13	–	–	–	121.58	121.53	121.62	–	–	–
C5–C4–C13	–	–	–	122.10	122.04	122.09	–	–	–
C4–C5–C13	121.16	121.39	122.2	–	–	–	–	–	–
C6–C5–C13	121.65	121.41	120.8	–	–	–	–	–	–
N8–C9–C14	–	–	–	–	–	–	116.49	116.55	116.12
C10–C9–C14	–	–	–	–	–	–	121.74	121.66	*
C9–C10–C14	–	–	–	121.58	121.59	121.62	–	–	–
C11–C10–C14	–	–	–	122.10	122.12	122.09	–	–	–
C10–C11–C14	121.16	121.26	121.2	–	–	–	–	–	–
C12–C11–C14	121.65	121.54	120.4	–	–	–	–	–	–
N2–C3–H1	116.02	116.05	118.4	115.79	115.82	117.4	–	–	–
C4–C3–H1	120.20	120.17	118.4	119.68	119.62	117.4	–	–	–
C3–C4–H1	–	–	–	–	–	–	120.21	120.19	*
C5–C4–H1	–	–	–	–	–	–	120.91	120.94	*
C3–C4–H2	119.98	119.99	120.0	–	–	–	–	–	–
C5–C4–H2	120.95	120.96	120.0	–	–	–	–	–	–

Table 2 (*continued*)

Geometric parameter	4DB			5DB			6DB		
	Calculated Value		Expt. Value[a]	Calculated Value		Expt. Value[b]	Calculated Value		Expt. Value[c]
	Monomer	Dimer		Monomer	Dimer		Monomer	Dimer	
C4–C5–H2	–	–	–	120.03	120.33	120.0	120.34	120.48	*
C6–C5–H2	–	–	–	119.93	119.91	120.0	120.35	120.13	*
C5–C6–H3	121.42	121.33	120.3	121.87	121.75	120.2	122.31	121.64	*
C1–C6–H3	118.68	118.71	120.3	119.19	119.05	120.2	119.37	120.13	*
N8–C9–H4	116.02	115.96	120.0	115.79	115.88	117.4	–	–	–
C10–C9–H4	120.20	120.57	120.0	119.68	119.49	117.4	–	–	–
C9–C10–H4	–	–	–	–	–	–	120.21	120.19	*
C11–C10–H4	–	–	–	–	–	–	120.91	120.94	*
C9–C10–H5	119.98	119.83	120.2	–	–	–	–	–	–
C11–C10–H5	120.96	120.92	120.2	–	–	–	–	–	–
C10–C11–H5	–	–	–	120.03	120.03	120.0	120.34	120.35	*
C12–C11–H5	–	–	–	119.93	119.95	120.0	120.35	120.34	*
C11–C12–H6	121.41	121.42	119.7	121.87	121.86	120.2	122.31	122.30	*
C7–C12–H6	118.67	118.71	119.7	119.19	119.10	120.2	119.37	119.31	*
C3–C13–H11	–	–	–	–	–	–	110.26	110.29	*
C3–C13–H12	–	–	–	–	–	–	111.72	110.28	*
C3–C13–H13	–	–	–	–	–	–	110.26	111.72	*
C4–C13–H11	–	–	–	111.26	111.21	109.5	–	–	–
C4–C13–H12	–	–	–	111.23	111.27	109.5	–	–	–
C4–C13–H13	–	–	–	111.26	111.21	109.5	–	–	–
C5–C13–H11	110.92	111.34	109.5	–	–	–	–	–	–
C5–C13–H12	111.38	111.35	109.5	–	–	–	–	–	–
C5–C13–H13	110.92	110.56	109.5	–	–	–	–	–	–
C9–C14–H21	–	–	–	–	–	–	110.26	110.51	*
C9–C14–H22	–	–	–	–	–	–	111.72	110.22	*
C9–C14–H23	–	–	–	–	–	–	110.26	111.67	*
C10–C14–H21	–	–	–	111.26	111.27	109.5	–	–	–
C10–C14–H22	–	–	–	111.23	111.26	109.5	–	–	–
C10–C14–H23	–	–	–	111.26	111.27	109.5	–	–	–
C11–C14–H21	110.94	111.14	109.5	–	–	–	–	–	–
C11–C14–H22	111.38	111.38	109.5	–	–	–	–	–	–
C11–C14–H23	110.90	110.71	109.5	–	–	–	–	–	–
H11–C13–H12	108.12	108.45	109.5	107.82	107.85	109.5	108.64	108.65	*
H12–C13–H13	108.12	107.62	109.5	107.82	107.85	109.5	108.64	108.60	*
H13–C13–H11	107.22	107.35	109.5	107.27	107.27	109.5	107.17	107.16	*
H21–C14–H22	108.14	108.32	109.5	107.82	107.80	109.5	108.64	108.66	*
H22–C14–H23	108.10	107.89	109.5	107.82	107.80	109.5	108.64	108.64	*
H23–C14–H21	107.22	107.24	109.5	107.27	107.26	109.5	107.17	106.99	*
Dihedral angle (in °)									
C1–N2–C3–C4	0.00	0.06	0.3	0.00	0.00	0.2	0.00	0.08	*
N2–C3–C4–C5	0.00	0.02	0.1	0.00	0.00	0.7	0.00	0.16	*
C3–C4–C5–C6	0.00	−0.07	−0.6	0.00	0.00	−0.9	0.00	−0.01	*
C4–C5–C6–C1	0.00	0.15	0.6	0.00	0.00	0.3	0.00	0.21	*
C5–C6–C1–N2	0.00	0.20	0.2	0.00	0.01	0.7	0.00	0.30	*
C6–C1–N2–C3	0.00	−0.14	−0.3	0.00	−0.01	−0.9	0.00	−0.15	*
C5–C6–C1–C7	−179.99	−179.70	−178.7	−179.99	−179.99	−179.66	−179.99	−179.74	*
C6–C1–C7–N8	−0.01	−4.32	*	0.00	−0.06	–	0.00	−2.40	*
C3–N2–C1–C7	179.99	179.66	179.3	179.99	179.99	179.44	179.99	179.89	*
N2–C1–C7–N8	179.99	176.16	*	179.99	179.95	–	179.99	177.64	*
C1–C7–N8–C9	179.99	179.38	180.0	180.00	179.99	–	179.99	179.79	*
C7–N8–C9–C10	0.00	0.21	0.1	0.000	0.00	0.2	0.00	0.35	*
N8–C9–C10–C11	0.00	0.06	0.6	0.000	0.00	0.7	0.00	0.06	*
C9–C10–C11–C12	−0.01	−0.24	−0.5	0.000	0.00	−0.9	0.00	−0.16	*
C10–C11–C12–C7	0.01	0.16	0.1	0.000	0.00	*	0.01	0.10	*
C11–C12–C7–N8	0.00	−0.11	−0.5	0.000	0.00	0.7	0.00	0.19	*
C11–C12–C7–C1	−179.99	−179.55	−180.0	−180.00	−180.00	−179.66	−179.99	−179.71	*
C12–C7–N8–C9	0.00	−0.29	−0.5	0.00	0.000	−0.9	0.00	−0.42	*
C12–C7–C1–N2	0.01	−4.16	*	0.00	−0.05	*	0.00	−2.45	*
C1–N2–C3–C13	–	–	–	–	–	–	179.99	179.90	*
C5–C4–C3–C13	–	–	–	–	–	–	−179.99	−179.82	*
N2–C3–C4–C13	–	–	–	180.00	179.99	179.06	–	–	–
C6–C5–C4–C13	–	–	–	−180.00	−179.99	−178.87	–	–	–
C3–C4–C5–C13	179.99	179.05	*	–	–	–	–	–	–
C1–C6–C5–C13	−179.99	−179.96	*	–	–	–	–	–	–
C1–N2–C3–H1	179.99	179.89	*	179.99	179.99	*	–	–	–
C5–C4–C3–H1	−179.99	−179.83	*	−179.99	−179.99	*	–	–	–
N2–C3–C4–H1	–	–	–	–	–	–	180.00	179.82	*
C6–C5–C4–H1	–	–	–	–	–	–	−179.99	−179.97	*
N2–C3–C4–H2	−180.00	−179.68	*	–	–	–	–	–	–
C6–C5–C4–H2	179.99	179.63	*	–	–	–	–	–	–
C3–C4–C5–H2	–	–	–	−179.99	−179.99	*	−179.99	−179.84	*

(*continued on next page*)

Table 2 (*continued*)

Geometric parameter	4DB			5DB			6DB		
	Calculated Value		Expt. Value[a]	Calculated Value		Expt. Value[b]	Calculated Value		Expt. Value[c]
	Monomer	Dimer		Monomer	Dimer		Monomer	Dimer	
C1–C6–C5–H2	–	–	–	179.99	179.99	*	179.99	179.62	*
C4–C5–C6–H3	179.99	179.39	*	180.00	179.99	*	180.00	179.97	*
N2–C1–C6–H3	−180.00	−179.36	*	−180.00	−179.99	*	−179.99	−179.94	*
C7–N8–C9–C14	–	–	–	–	–	–	179.99	179.47	178.7
C11–C10–C9–C14	–	–	–	–	–	–	−179.99	−179.95	*
N8–C9–C10–C14	–	–	–	−180.00	−179.99	*	–	–	–
C12–C11–C10–C14	–	–	–	180.00	179.99	*	–	–	–
C9–C10–C11–C14	179.94	179.28	*	–	–	–	–	–	–
C7–C12–C11–C14	−179.94	−179.36	*	–	–	–	–	–	–
C7–N8–C9–H4	−179.99	−179.89	*	−179.99	−179.99	*	–	–	–
C11–C10–C9–H4	179.99	179.84	*	179.00	179.99	*	–	–	–
N8–C9–C10–H4	−179.99	−179.98	*	–	–	–	−179.99	−179.95	*
C12–C11–C10–H4	179.98	179.84	*	–	–	–	179.99	179.82	*
C9–C10–C11–H5	–	–	–	−179.99	−179.99	*	−179.99	−179.95	*
C7–C12–C11–H5	–	–	–	179.99	179.99	*	179.99	179.99	*
C10–C11–C12–H6	−179.98	−179.76	*	−180.00	−179.99	*	−179.99	−179.88	*
N8–C7–C12–H6	179.98	179.97	*	180.00	179.99	*	180.00	179.83	*

Inter-molecular H-bond length and bond angle of Dimers

Geometric parameter	Bond length (in Å)			Bond Angle (in °)		
	4DB	5DB	6DB	4DB	5DB	6DB
C1′-N2'·····H4	2.710	–	–	147.09	–	–
C7–N8·····H1′	2.706	–	–	147.01	–	–
C1′-N2'·····H2	–	3.306	–	–	137.62	–
C7–N8·····H5′	–	3.346	–	–	137.80	–
C1′-N2'·····H3	–	–	2.990	–	–	120.07
C7–N8·····H6′	–	–	2.990	–	–	120.07

-: Not relevant.
*: Not available.
[a] From Ref. 13.
[b] From Ref. 14.
[c] From Ref. 15.

hydrogen bond lengths and minimum energy. The optimized structure parameters those include bond lengths, bond angles and dihedral angles, for both monomers and dimers of 4DB, 5DB and 6DB are given in Table 2. The parameters connected with inter-molecular hydrogen bond of dimers are also shown in the same Table. The theoretically calculated parameters are also compared in Table 2 with their corresponding experimental values obtained from XRD analyses [13–15].

4.1.1. Monomer and dimer

It was observed in the previous section that the three molecules under investigation assume C_1 symmetry. From Table 2, it is evident that the theoretical structure parameters of 4DB, 5DB and 6DB agree reasonably with their corresponding experimental values obtained from X-ray diffraction studies [13–15]. For example, according to the computations for 4DB, the average value of intra-ring C–C bond length is 1.395 Å; the average value of C–N bond distance is 1.337 Å; the average value of C–H bond distance associated with the bipyridine unit, is 1.085 Å; the average value of aromatic–methyl C–C bond (i.e., C-C_α bond) is estimated to be 1.507 Å; inter-ring C–C bond is predicted at 1.492 Å; and the average value of C_α-H bond measures 1.093 Å. They agree remarkably well with their corresponding X-ray diffraction values 1.385 Å; 1.341 Å; 0.930 Å; 1.500 Å; 1.479 Å and 0.960 Å in 4DB [13]. Similarly, the average value of intra-ring C–C bond length; the average value of C–N bond distance; the average value of aromatic-methyl C–C bond and inter-ring C–C bonds measures, 1.396 Å and 1.395 Å; 1.336 Å and 1.339 Å for 5DB; and 1.489 Å and 1.493 Å; and 1.506 Å and 1.507 Å for 6DB respectively, and their corresponding experimental values are 1.383 Å and 1.384 Å; 1.337 Å and 1.345 Å for 5DB [14]; and 1.491 Å and 1.485 Å; and 1.511 Å and 1.503 Å [15], respectively.

Some bond angles in bipyridine ring with nitrogen atom are ∠C1N2C3, ∠N2C3C4, ∠C7N8C9 and ∠N8C9C10 having calculated values 117.67°, 123.77°, 117.69° and 123.77°, respectively for 4DB, which agree fairly well with X-ray diffraction results [13] at 116.7°,123.2°, 119.9° and 123.4°. Similar conclusions can be observed from Table 2 for 5DB and 6DB.

The dimer of 4DB, 5DB, and 6DB was considered as a supramolecule containing two equilibrium monomers in their minimum energy conformation separated by a distance favorable for intermolecular hydrogen bond formation between nitrogen atom of pyridine ring of one monomer and hydrogen atom of the pyridine ring of another monomer. This initial distance, to be specific, was 1.557 Å, 1.500 Å and 2.282 Å for 4DB, 5DB and 6DB, respectively. The resulting structure was subjected to rigorous geometry optimization by relaxing all structure parameters simultaneously as in the case of monomer. This process yielded structure of C_1 symmetry for the dimers of 4DB, 5DB and 6DB. As both the monomer and the dimer are considered at the same level of theory, comparative results are predictable to be trustworthy.

The minimum energy of 4DB, 5DB and 6DB dimers is computed as -3014.972×10^3, -3014.962×10^3 and -3014.988×10^3 kJmol^{-1}, respectively. To ascertain that the resultant dimeric structure of the three molecules is reliable, the minimum energy should be less than twice the minimum energy of corresponding monomers. It can be observed that the difference between the minimum energy of 4DB dimer and twice the energy of its monomer is −6 kJmol^{-1}.

Table 3
Summary of vibrational assignments, observed and calculated (Un-scaled and Scaled) frequencies (in cm^{-1}) of 4DB, 5DB and 6DB.

Mode[a]	4DB				5DB				6DB			
	Obs. freq.		.Cal. freq.		Obs. freq		Cal. freq.		Obs. freq.		Cal. freq.	
	IR	Raman	Un-scaled	scaled	IR	Raman	Un-scaled	Scaled	IR	Raman	Un-Scaled	Scaled
(i) Vibrations of Bipyridine												
(a) In-plane vibrations												
ν(C–N)1	989	995	1023	992	975	–	1045	979	987	992	1010	983
ν(C–C)8a	–	1605	1641	1609	–	1625	1640	1626	–	1598	1620	1597
ν(C–N)8b	1559	1560	1595	1553	1595	1595	1613	1597	1573	1572	1610	1561
ν(C–C)14	1248	1236	1283	1240	–	–	1323	1312	–	1315	1332	1314
ν(C–C)19a	–	–	1519	1511	–	1497	1525	1511	–	–	1468	1462
ν(C–C)19b	–	1436	1454	1433	–	–	1420	1408	–	–	1464	1412
ν(C–N)1′	989	995	1012	982	975	–	1046	1005	987	992	1018	1004
ν(C–C)8a′	–	1605	1634	1600	–	1625	1631	1608	–	1626	1633	1619
ν(C–N)8b′	1559	1560	1599	1574	1552	–	1583	1562	–	–	1612	1594
ν(C–C)14′	1248	1236	1284	1258	–	–	1274	1251	1245	1255	1289	1261
ν(C–C)19a′	–	–	1495	1478	–	1497	1503	1487	–	–	1490	1474
ν(C–C)19b′	–	–	1397	1375	–	–	1403	1387	–	–	1419	1381
ν(C–H)2	3053	3055	3203	3083	–	3061	3213	3080	3060	3068	3221	3066
ν(C–H)20a	–	–	3173	3054	3031	3034	3157	3042	–	3040	3185	3032
ν(C–H)20b	3024	–	3142	3018	3007	3014	3132	3001	–	3004	3166	3014
ν(C–H)2′	3053	3055	3204	3085	–	3061	3214	3079	3060	3068	3220	3067
ν(C–H)20a′	–	–	3173	3054	3031	3034	3157	3038	–	3040	3185	3032
ν(C–H)20b′	3024	–	3143	3018	3007	3014	3132	3001	–	3004	3166	3014
ν(C-$C_α$)7b	–	–	1239	1221	–	–	1243	1235	–	–	1247	1206
ν(C-$C_α$)7b′	–	1159	1179	1166	1218	1226	1239	1229	–	–	1262	1232
ν(C–C′)13	–	735	748	731	650	–	682	658	–	692	704	689
β(CH)3	–	–	1316	1305	–	–	1343	1327	–	–	1304	1290
β(CH)18a	1068	–	1095	1079	–	–	1078	1069	–	–	1105	1053
β(CH)18b	–	–	1134	1119	–	–	1155	1147	1112	–	1175	1110
β(CC′)15	–	–	121	121	–	–	121	120	–	–	123	118
β(C$C_α$)9a	–	340	364	342	–	–	353	344	–	344	381	347
β(CH)3′	–	1317	1342	1330	–	–	1316	1296	1151	1158	1178	1160
β(CH)18a′	–	1111	1132	1112	1127	1124	1150	1137	1079	1083	1108	1095
β(CH)18b′	1273	1286	1312	1287	1268	–	1275	1267	–	–	1133	1099
β(C'C)15′	–	–	475	467	465	468	475	467	–	–	482	463
β(C$C_α$)9a′	–	238	249	237	–	285	296	289	–	240	257	241
β(CCC)6a	–	–	345	332	–	–	285	272	–	–	341	333
β(CCC)6b	–	–	533	529	–	–	642	599	548	557	563	556
β(CCC)12	822	–	834	817	795	–	812	787	–	819	825	809
β(CCC)6a′	–	–	530	509	–	–	548	515	–	–	558	537
β(CCC)6b′	668	–	687	664	–	629	667	626	632	–	651	630
β(CCC)12′	911	917	931	911	827	836	846	827	908	914	926	905
(b) Out-of plane vibrations												
π(CH)5	965	–	984	965	–	–	1007	1004	–	–	1015	1003
π(CH)11	–	–	852	842	–	862	885	861	–	–	843	840
π(CH)17b	–	–	947	925	–	–	940	938	–	–	936	927
π(CH)5′	–	–	983	938	–	–	1003	948	–	–	1014	994
π(CH)11′	–	–	837	811	–	–	849	819	780	–	797	785
π(CH)17b′	–	–	931	897	–	–	939	892	–	–	925	911
π(C$C_α$)10a	–	–	626	613	–	535	565	547	–	–	647	625
π(CC′)10b	514	524	528	518	–	–	479	470	521	–	534	519
π(C$C_α$)10a′	–	–	216	210	–	–	259	255	–	208	236	230
π(C'C)10b′	–	77	92	92	–	–	52	51	–	72	96	95
τ(CCCC)4	–	–	754	730	735	–	755	735	–	–	762	760
τ(CCCC)16a	–	–	203	178	–	–	131	130	–	–	204	199
τ(CCCC)16b	–	–	423	341	–	–	415	384	–	–	449	446
τ(CCCC)4′	–	–	786	780	–	769	788	765	734	–	754	734
τ(CCCC)16a′	–	–	228	222	–	–	352	343	–	–	198	188
τ(CCCC)16b′	–	–	467	462	–	412	425	411	–	–	436	413
τ(CC′)	–	–	35	34	–	–	51	53	–	–	32	30
(ii) Methyl groups												
(a) In-plane vibrations												
$ν_s(CH_3)_1$	2855	–	3028	2855	2859	–	3023	2858	2853	–	3033	2853
$ν_{as}(CH_3)_{ip1}$	2992	–	3111	2981	2954	2954	3157	2954	2946	–	3111	2946
$δ_{as}(CH_3)_{ip1}$	–	1480	1491	1480	1465	1454	1498	1472	1437	–	1478	1437
$δ_s(CH_3)_1$	1366	–	1412	1365	–	1389	1417	1391	1368	1377	1410	1370
$γ(CH_3)_{ip1}$	965	–	1007	960	930	935	1006	937	987	992	1036	991
$ν_s(CH_3)_2$	2855	–	3028	2855	2859	–	3023	2860	2853	–	3033	2853
$ν_{as}(CH_3)_{ip2}$	2992	–	3111	2981	2954	2954	3157	2955	2946	–	3111	2947
$δ_{as}(CH_3)_{ip2}$	–	1480	1494	1483	1465	1454	1492	1467	1437	–	1478	1438
$δ_s(CH_3)_2$	1366	–	1412	1364	–	1389	1416	1389	1368	1377	1406	1366
$γ(CH_3)_{ip2}$	965	–	1009	969	930	935	1005	935	–	–	996	961
(b) Out-of plane vibrations												

(*continued on next page*)

Table 3 (*continued*)

Mode[a]	4DB				5DB				6DB			
	Obs. freq.		.Cal. freq.		Obs. freq		Cal. freq.		Obs. freq.		Cal. freq.	
	IR	Raman	Un-scaled	scaled	IR	Raman	Un-scaled	Scaled	IR	Raman	Un-Scaled	Scaled
$\nu_{as}(CH_3)_{op1}$	2919	2920	3078	2922	2918	2921	3072	2917	2919	–	3089	2919
$\delta_{as}(CH_3)_{op1}$	1455	–	1487	1455	1465	1454	1487	1459	–	1463	1495	1450
$\gamma(CH_3)_{op1}$	1044	1037	1063	1038	1030	1049	1062	1040	1036	–	1058	1035
$\nu_{as}(CH_3)_{op2}$	2919	2920	3078	2922	2918	2921	3072	2921	2919	–	3089	2919
$\delta_{as}(CH_3)_{op2}$	1455	–	1487	1455	1465	1454	1487	1444	–	1463	1502	1457
$\gamma(CH_3)_{op2}$	1044	1037	1063	1039	1030	1049	1062	1037	1036	–	1059	1037
$\tau(CH_3)_1$	–	–	31	31	–	–	72	72	–	–	64	62
$\tau(CH_3)_2$	–	–	32	32	–	–	64	64	–	–	62	58

-: Not observed.

[a] Mode in Wilson's notation [43]. Prime (') on the mode (in Wilson's notation) refers to the modes associated with the second pyridyl ring and C_α refers to Carbon atom of methyl group; ν, stretching; β, in-plane bending; δ, deformation; γ, rocking; π, out-of-plane bending; τ, torsion; s, symmetric; as, asymmetric; ip, in-plane; op, out-of-plane.

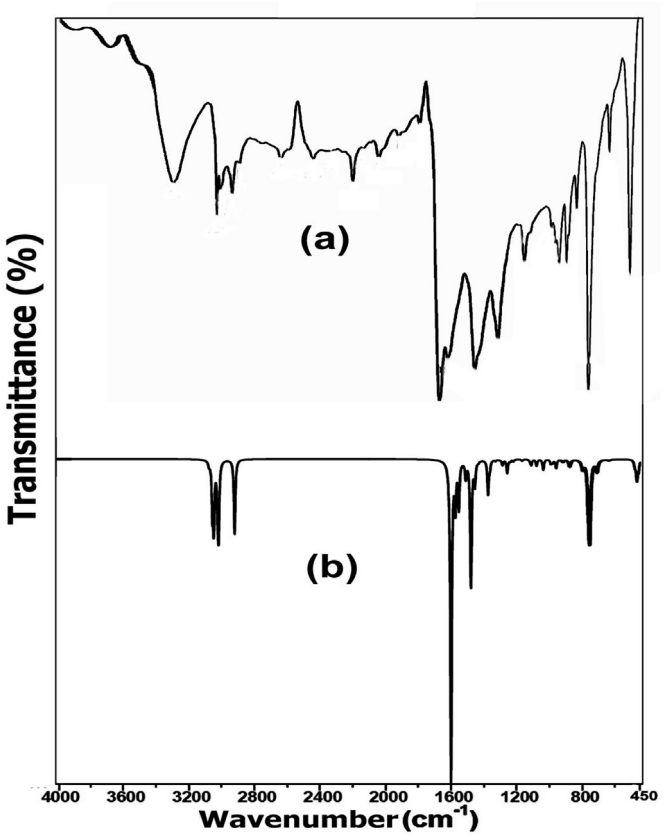

Fig. 6. FT-IR Spectrum of 4DB (a) Experimental and (b) Simulated with. DFT/B3LYP/6-311++G(d,p) formalism.

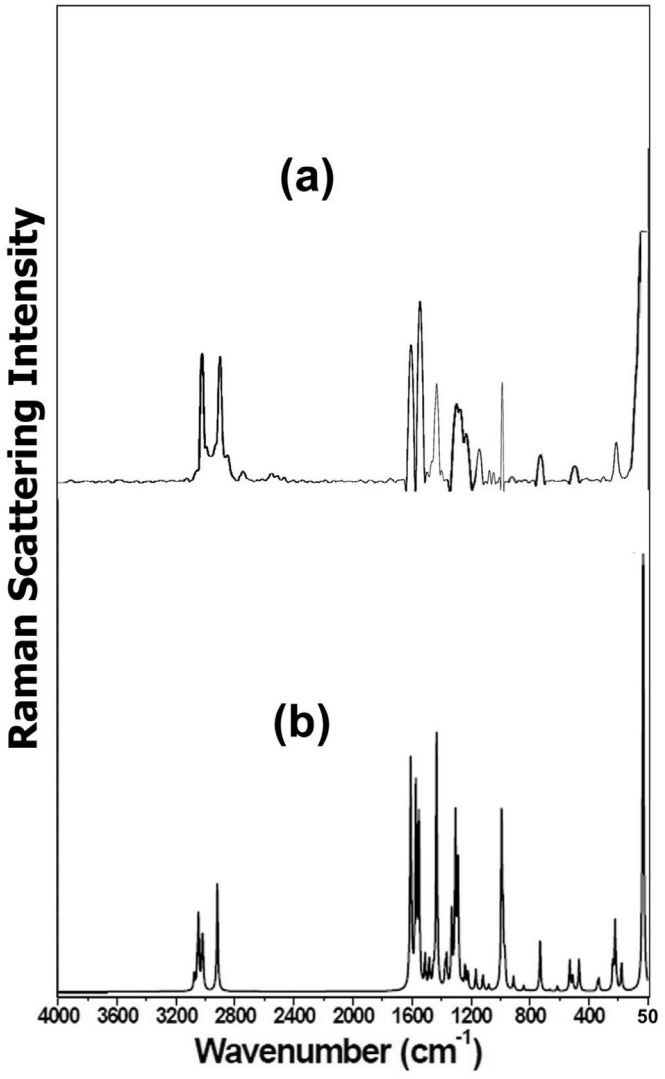

Fig. 7. FT-Raman Spectrum of 4DB (a) Experimental and (b) Simulated with DFT/B3LYP/6-311++G(d,p) formalism.

Similarly, the corresponding energy difference of 5DB and 6DB dimers is −4 kJmol^{-1} and -4 kJmol^{-1}, respectively. Hence, the optimized monomers of 4DB, 5DB and 6DB tend to form corresponding dimers.

In dimers of 4DB, 5DB and 6DB structural configuration, the formation of inter-molecular hydrogen bond is of special interest (see Fig. 5). The relevant bond distances and bond angles are available in Table 2. From Fig. 5 and Table 2, it could be observed that for 4DB dimer, the calculated hydrogen bond lengths are: H1′·····N8 = 2.706 Å and N2′·····H4 = 2.710 Å. Corresponding quantities for 5DB dimer are: N2′····H2 = 3.306 Å and H5′·····N8 = 3.346 Å, whereas they are N2′·····H3 = 2.990 Å and H6′·····N8 = 2.990 Å, for 6DB dimer (here,′ indicates second monomer in three dimers). According to Steiner's review article [38], hydrogen bonds, generally, comprise of different types of interactions, but in the medium and long-distance region, the electrostatic component is the dominant one. Steiner [38] also

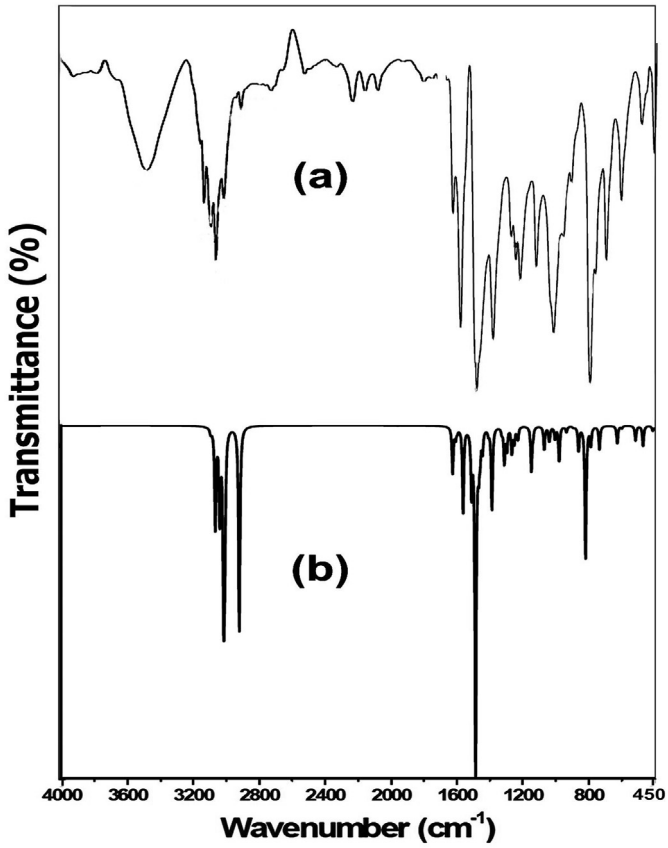

Fig. 8. FT-IR Spectrum of 5DB (a) Experimental and (b) Simulated with DFT/B3LYP/6-311++G(d,p) formalism.

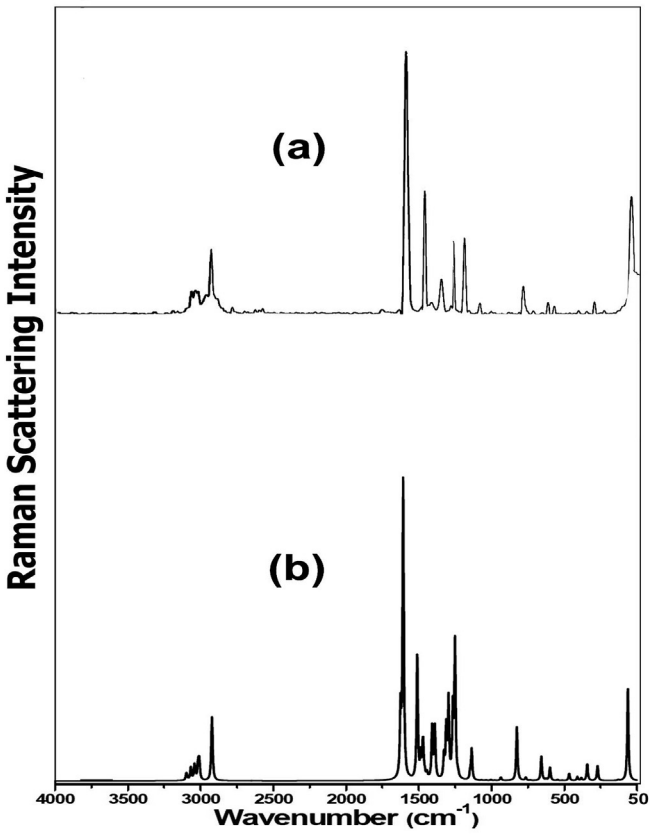

Fig. 9. FT-Raman Spectrum of 5DB (a) Experimental and (b) Simulated with DFT/B3LYP/6-311++G(d,p) formalism.

suggested that the hydrogen bonds having bond distances in the range 2.4–2.8 Å are weak. As the computed bond distance in 4DB dimer fall in range 2.4–2.8 Å and hence, they may be considered as weak. The bond lengths in 5DB and 6DB dimers are >2.8 Å and thus, they are thought to form by weak Van der Waals interactions arising from electrostatic forces. As proposed by Steiner and Desiraju [39,40], it is not easy to ascertain where a hydrogen bond ceases and a Van der Waals interaction instigates. However, hydrogen bond interactions may be assessed in a better manner by using Bader's theory of 'Atoms in Molecules' implemented in AIM2000 software updated by Biegler-könig and Schönbohm [41] in 2002.

4.2. Vibrational assignments

All force constants of general valence force field were evaluated for 4DB, 5DB and 6DB using DFT/B3LYP/6-311++G(d,p) method for solving the secular equation employing Willson's GF matrix method [42]. In DFT computations, the number of actual vibrations of a non-linear molecule given by 3N−6 (N is the number of atoms) is equal to the number of natural internal coordinates. The three molecules 4DB, 5DB and 6DB consist of 26 atoms each. Hence, the number of genuine vibrations n = 3N-6 = 72 for each one of them. The molecules under investigation belong to C_1 point group symmetry having only one type of symmetry species (i.e., a-species) and are active in infrared and Raman spectrum.

Vibrational modes designated in Wilson's notation [43], experimental (both infrared and Raman) and calculated (both un-scaled and scaled) frequencies of 4DB, 5DB and 6DB are summarized in Table 3, whereas the computed IR and Raman intensities, potential energy distribution (PED) and vibrational assignments of the three molecules are presented in Tables S1–S3 as supplementary material. Some absorption peaks in both FTIR and Raman spectra are observed in the spectral region 1700-2800 cm^{-1} for the three molecules. These absorption peaks were considered as overtones and combinational bands. They are presented in Table S4 as supplementary material. A visual comparison of experimental and simulated FT-IR and FT- Raman spectra is made in Figs. 6–11, respectively.

The rms error is calculated as 9.20, 8.21 and 8.33 cm^{-1} between experimental and scaled frequencies for 4DB, 5DB and 6DB, respectively. Linear regression curves between experimental and calculated frequencies are plotted for the three molecules and are shown in Fig. 12. The regression coefficient (r^2) is determined as 0.99 for the three molecules. The value of rms error and regression coefficient demonstrates that the frequency fit between the experimental and calculated frequencies may be considered as good which can be realized from Table 3 and Fig. 12. Hence, the vibrational assignments made based on the PED obtained in DFT computations for 4DB, 5DB and 6DB are unambiguous.

The results presented in Table 3 and supplementary Tables S1–S3 are self-explanatory. Hence, the discussion of vibrational assignment is mainly confined to the fundamentals originating from the pyridine ring substituted with methyl group.

4.2.1. C–C and C–N stretching vibrations of pyridine rings

The modes 1, 8a, 8b, 14, 19a and 19b (Wilson's notation is used for benzene ring modes) [43] are known as C–C stretching

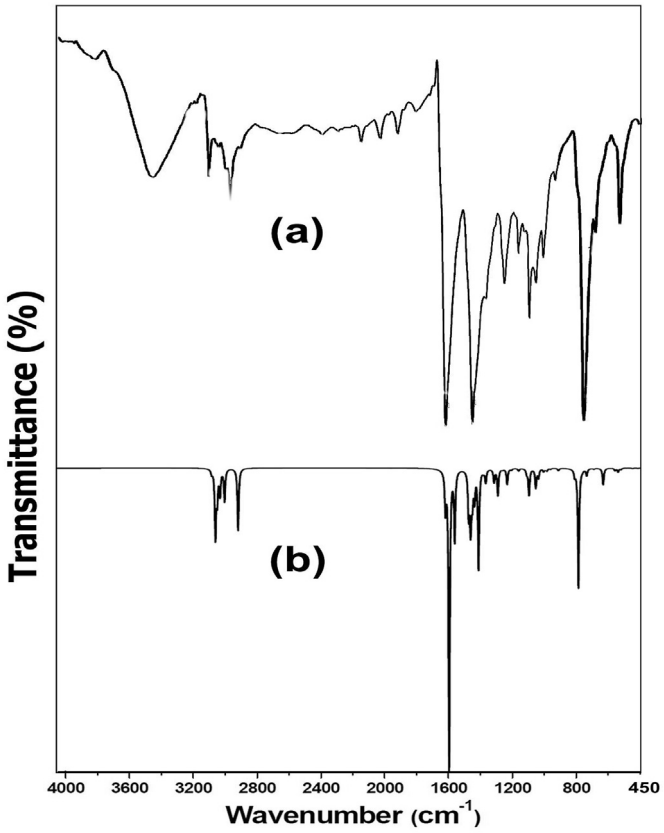

Fig. 10. FT-IR Spectrum of 6DB (a) Experimental and (b) Simulated with DFT/B3LYP/6-311++G(d,p) formalism.

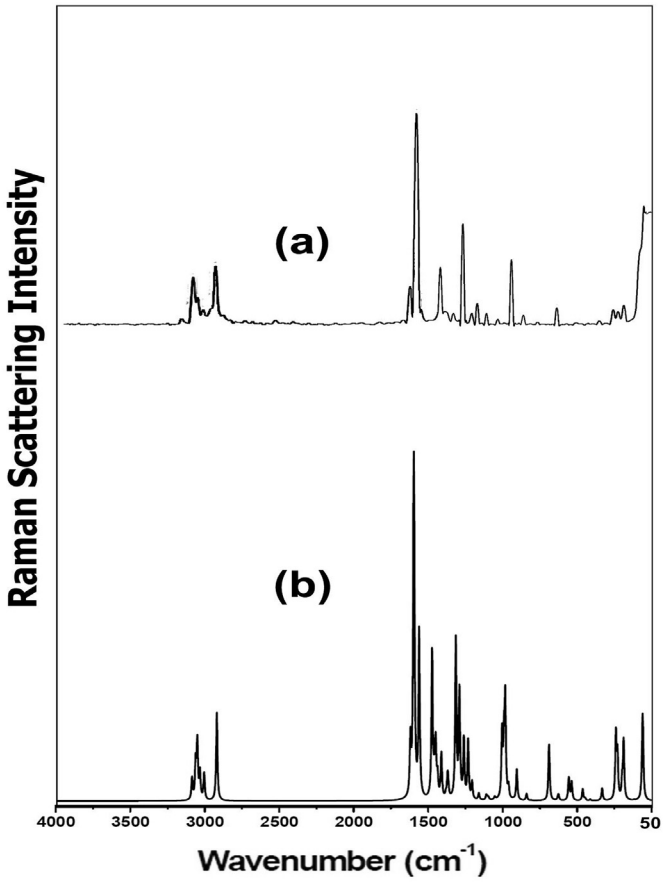

Fig. 11. FT-Raman Spectrum of 6DB (a) Experimental and (b) Simulated with DFT/B3LYP/6-311++G(d,p) formalism.

vibrations in benzene and its derivatives. Each of the three samples under investigation contains two nitrogen atoms and ten carbon atoms in aromatic nucleus. Hence, we get eight C—C and four C—N stretching vibrations for each of the three molecules under investigation. The modes 8a, 14, 19a, and 19b correspond to the C—C stretching vibrations of one pyridine ring and 8a′, 14′, 19a′ and 19b′ are C—C stretching vibrations of other pyridine ring, whereas the modes 1, 1′, 8b and 8b′ represent C—N stretching vibrations in these molecules. For the molecules 4DB, 5DB and 6DB, the modes 8a and 8b are expected around 1550-1600 cm^{-1} as suggested by Varsanyi [44] for benzene and its derivatives. The pair of higher frequency has PED to the extent 31% and 45%; 62% and 57%; and 69% and 55% from the C—C stretching mode 8a and 8a′ in 4DB, 5DB and 6DB, respectively, which can be seen from supplementary Tables S1—S3. The remaining PED comes from C—H in-plane bending modes 18b and 18b′ in 4DB and 5DB, whereas, such mixing arises from 18a and 18a′ in 6DB. There is an additional PED contribution to this fundamental from ∠CCC bending modes 12 and 12′ in 4DB and 5DB, whereas such contribution comes from vibration 6a and 6a′ in 6DB. C—N stretching vibration represented by mode 8b and 8b′ has PED to the extent of 59% and 70%; 47% and 47%; and 64% and 68% in these molecules and mixes with C—H in-plane bending vibrations and ∠CCC bending modes as can be seen from Tables S1—S3. According to the computations made here, the frequency of mode 8a is higher than that of vibration 8b. Hence, the absorption bands near 1605R (R indicates Raman shift), 1625R cm^{-1} are ascribed to modes 8a and 8a′ in both 4DB and 5DB, respectively, whereas, the frequencies near 1598R and 1626R cm^{-1} are assigned to mode 8a and 8a′ in 6DB, respectively. IR bands near 1559, 1595 and 1573 cm^{-1} are assigned to vibration 8b, whereas, those at 1559, 1552 and 1594C cm^{-1} (C indicates scaled calculated value) are attributed to mode 8b′ in 4DB, 5DB and 6DB, respectively.

Modes 19a and 19b are expected in the spectral range 1400—1500 cm^{-1} as proposed by Varsanyi [44] for seven hundred benzene derivatives. The higher frequency has C—C stretching character ranging from 28% to 37% in the three molecules. It exhibits strong mixing with C—H in plane bending mode 18b in 4DB, 5DB and 6DB. Considerable contribution of PED exists in this mode from 18a′ (8%) in 4DB, 13 (11%) in 5DB, whereas, in 6DB, out of plane deformation mode of methyl group δ_{op} contributes 7% PED to 19 mode and 12% PED to 19a′ mode in 6DB. The lower frequency exhibits C—C stretching character to the extent from 19% to 41%. It mixes with C—H in-plane bending vibration mode 3 in all three molecules. There is an additional PED contribution to this mode from 13 in 4DB and 6DB, whereas mode 9a in 5DB. In addition, in-plane deformation bending mode of methyl group δ_{ip} exists in 4DB and 5DB. Thus, the absorptions near 1497R cm^{-1} is ascribed as mode 19a and 19a′ in 5DB; 1511C and 1478C; and 1462C and 1474C cm^{-1} are assigned to mode 19a and 19a′, in 4DB and 6DB, respectively, while the frequencies obtained at 1436R and 1375C cm^{-1}; 1408C and 1387C cm^{-1}; and 1412C and 1381C cm^{-1} are attributed to the modes 19b and 19b′ in 4DB, 5DB and 6DB, respectively.

Mode 14 is characterized by, either increase or decrease of alternate carbon bonds of the ring. This vibration is known to mix strongly with C—H bending mode 3 in a number of substituted benzenes. This mode appears at 1248, is assigned to mode 14 and 14′ in 4DB, whereas, 1312C and 1251C cm^{-1}; and 1315R and 1245 are ascribed to 14 and 14′ modes in 5DB and 6DB, respectively. This

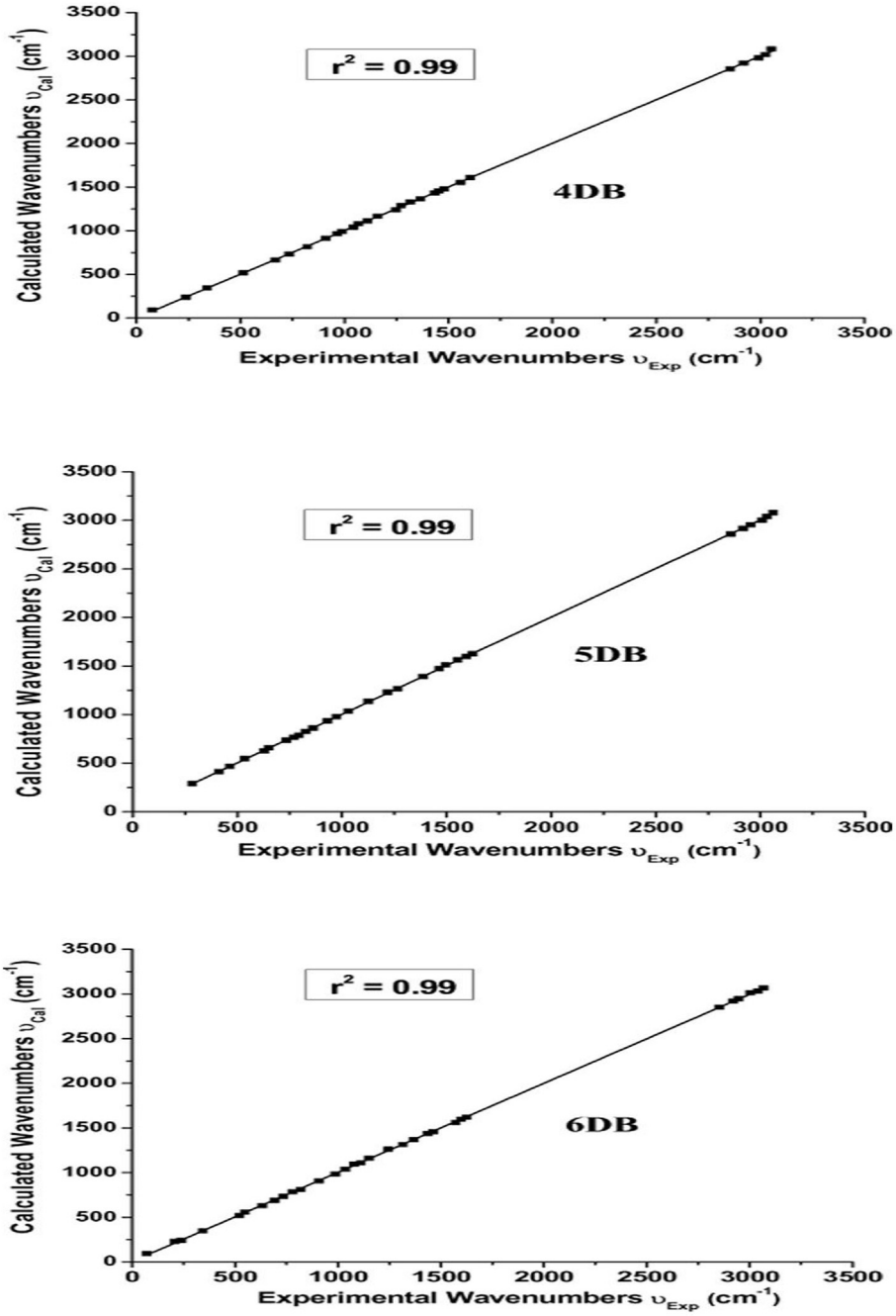

Fig. 12. Linear regression curves between the observed and calculated frequencies for 4DB, 5DB and 6DB.

mode has C—C stretching character in the range 56—79%.

4.2.2. C—H in-plane bending vibrations of pyridine rings

The modes 3 and 3′ are observed at 1305C and 1317R cm^{-1} in 4DB, which has 24% and 18% PED from C—H in-plane bending character. Similarly, the absorptions at 1327C and 1296C cm^{-1} having PED of 48% and 9% and 1290C and 1151 cm^{-1}, PED contribution of 48% and 9%; and 9% and 82% are ascribed to modes 3 and 3′, in 5DB and 6DB, respectively. As expected, this mode 3 mixes with vibration 14 in three molecules. In addition, it mixes with mode 14′ in 4DB to the extent of 24%, whereas, such mixing of PED to the extent of 15% can be seen in 6DB. It is to be noted that, this mode in three molecules mixes with vibrational mode 13.

According to calculations, the pair of bands near 1068 and 1111R cm^{-1}; 1069C and 1127 cm^{-1}; and 1053C and 1079 cm^{-1} are identified as C—H bending modes 18a and 18a′, in 4DB, 5DB and 6DB, respectively, while the frequencies obtained at 1119C and 1273 cm^{-1}; 1147C and 1268 cm^{-1}; and 1112 and 1099C cm^{-1} are attributed to the modes 18b and 18b′ in the molecules 4DB, 5DB and 6DB, respectively. Both these vibrations mix with C—C/C—N stretching and ∠CCC bending modes, which can be seen in Tables S1—S3.

The vibrational assignments of C—H stretching vibrations, ring or substituent sensitive modes, ring torsions, C—H out-of-plane bending vibrations, vibrations associated with the inter-ring C—C bond and vibrations of C-C_α (bond between pyridine ring and

Table 4
Experimental and theoretical ^{1}H and ^{13}C NMR chemical shifts δ (ppm) of 4DB, 5DB and 6DB.

Atom	4DB		5DB		6DB	
	Experimental	Calculated	Experimental	Calculated	Experimental	Calculated
H1	8.23	8.66	8.23	8.62	7.67	7.83
H2	7.13	7.30	7.60	7.86	7.14	7.24
H11	2.43	2.57	2.36	2.38	2.62	2.72
H12	2.43	2.17	2.36	2.13	2.62	2.25
H13	2.43	2.57	2.36	2.38	2.62	2.72
H3	8.54	8.91	8.48	8.86	8.18	8.76
H4	8.23	8.66	8.23	8.62	7.67	7.83
H5	7.13	7.30	7.60	7.86	7.14	7.24
H21	2.43	2.57	2.36	2.38	2.62	2.72
H22	2.43	2.17	2.36	2.13	2.62	2.25
H23	2.43	2.57	2.36	2.38	2.62	2.72
H6	8.54	8.92	8.48	8.86	8.18	8.76
C1	155.89	162.54	153.63	160.04	155.84	161.69
C3	148.14	153.49	149.41	154.01	157.79	165.12
C4	124.60	129.13	132.91	140.09	123.01	127.08
C5	148.82	155.21	137.31	142.07	136.96	141.95
C6	121.98	125.45	120.20	123.86	118.14	121.08
C7	155.89	162.54	153.63	160.04	155.84	161.69
C9	148.14	153.49	149.41	154.01	157.79	165.12
C10	124.60	129.13	132.91	140.09	123.01	127.08
C11	148.82	155.21	137.31	142.07	136.96	141.95
C12	121.98	125.54	120.20	123.86	118.14	121.08
C13	21.13	21.82	18.21	18.08	24.61	25.47
C14	21.13	21.82	18.21	18.08	24.61	25.47

methyl group) are made unambiguously using PED and eigen vectors obtained in the DFT computations as discussed in our earlier paper on bipyridines [10], whereas the vibrational assignments of two methyl groups are made on the same lines as presented in our earlier work on dimethylanilines [45]. PED % in each mode of vibration and mixing of modes in 4DB, 5DB and 6DB can be easily understood from supplementary Tables S1–S3. Hence, detailed discussion is unwarranted.

4.3. Assignment of NMR signals

It is known that NMR signals depend on chemical environment of a given atom. In three titled compounds, the two methyl pyridine rings are symmetric in nature (see Fig. 4). Hence, ^{1}H NMR and ^{13}C NMR spectra of 4DB, 5DB and 6DB are recorded. Theoretical and experimental chemical shifts in ^{13}C and ^{1}H NMR spectra of these molecules are presented in Table 4. ^{1}H NMR spectra of the samples are presented in Fig. 13, whereas their ^{13}C NMR counterparts are presented in Fig. 14. It can be seen from Fig. 13 that there are 4 proton signals corresponding to the twelve hydrogen atoms in each of the three molecules, three proton signals are for aromatic hydrogens and one proton signal is for methyl group hydrogens. They are assigned as shown below.

4DB: ^{1}H NMR (CDCl3, 500 MHz): $\delta = 8.54$ (d, $J = 5$ Hz, 2H), 8.23 (m, 2H), 7.13 (m, 2H) and 2.43 (s, CH3 group) ppm.

5DB: ^{1}H NMR (CDCl3, 500 MHz): $\delta = 8.48$ (m, 2H), 8.23 (d, j = 8 Hz, 2H), 7.60 (m, 2H) and 2.36 (s, CH3 group) ppm.

6DB: ^{1}H NMR (CDCl3, 500 MHz): $\delta = 8.18$ (d, $J = 8$ Hz, 2H), 7.67 (t, $J = 8$ Hz, 2H),7.14 (d, $J = 8$ Hz, 2H) and 2.62 (s, CH3 group) ppm.

4DB, 5DB and 6DB consist of twelve carbon atoms each. Ten of these are aromatic carbon atoms associated with bipyridine unit and two carbonyl carbon atoms belonging to the methyl group. Hence, we expect twelve distinct ^{13}C chemical shifts in each of their ^{13}C NMR spectra, whereas, from ^{13}C NMR spectra only six spectral lines are observed. This may not be true always as some of the aromatic carbons give signals in overlapped areas of the spectrum with chemical shift values from 100 to 150 ppm [46]. This overlapping causes a reduction in the number of distinct ^{13}C NMR signals. This is found true in ^{13}C NMR spectra of 4DB, 5DB and 6DB as the number of corresponding signals are six, instead of expected twelve. They are assigned below.

4DB: ^{13}C NMR (CDCl3, 500 MHz): $\delta = 155.89$, 148.82, 148.14, 124.60, 121.98 (aromatic carbons), 21.13(Methyl group) ppm.

5DB: ^{13}C NMR (CDCl3, 500 MHz): $\delta = 153.63$, 149.41, 137.31, 132.91, 120.20 (aromatic carbons), 18.21(Methyl group) ppm.

6DB: ^{13}C NMR (CDCl3, 500 MHz): $\delta = 157.79$, 155.84, 136.96, 123.01, 118.14 (aromatic carbons), 24.61(Methyl group) ppm.

In order to verify the agreement between the simulated and experimental NMR signals, plots are drawn with experimental chemical shifts vs calculated chemical shifts for 4DB, 5DB and 6DB. This yielded straight lines as shown in Figs. 15 and 16 for ^{1}H and ^{13}C NMR spectra, respectively. The value of correlation coefficient (r^2) is found to be close to unity for both ^{1}H NMR and ^{13}C NMR spectra of the three molecules being treated (see Figs. 15 and 16). This demonstrates good agreement between the experimental and theoretical chemical shifts.

It is important to note here that the NMR signals around 7.26–7.28 ppm in ^{1}H NMR spectra (see Fig. 13) and around 77.00 ppm in ^{13}C NMR spectra of these molecules (see Fig. 14) is resulted due to the carbon atom of solvent $CDCl_3$ and its fine structure are attributable to isotope shift.

4.4. Frontier molecular orbitals

The molecules under investigation were considered to possess frontier orbitals which are merely the highest occupied molecular orbital (HOMO) and lowest unoccupied molecular orbital (LUMO). These frontier molecular orbitals were subjected to determine the kinetic characteristics of reactants and reactions. Orbital overlap between HOMO and LUMO will be maximum, when the separation between them is greater than some typical bond lengths and leads to the main interactions as reactants approach. HOMO and LUMO are used to evaluate the frontier electron density for calculating the most reactive position in π-electron systems. The gap between

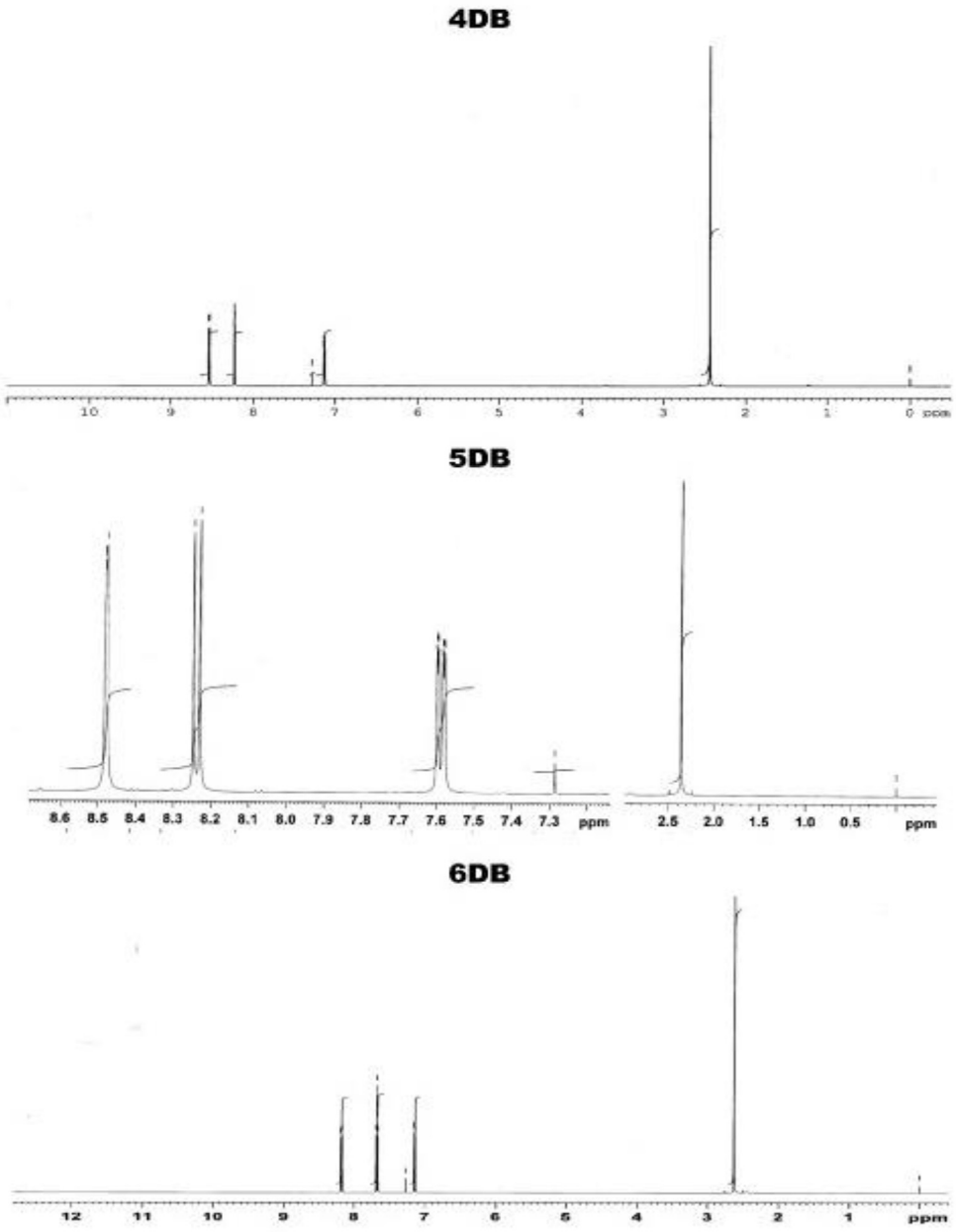

Fig. 13. Experimental ^{1}H NMR spectra of 4BD, 5DB and 6DB.

HOMO and LUMO illustrates the chemical stability of a molecule. A small gap designates the significant degree of intermolecular charge transfer from electron-donor groups to the efficient electron-accepter groups through π-conjugated path [47].

The energies of HOMO, LUMO and frontier molecular orbital gap at DFT/B3LYP/6-311++G(d,p) level of theory for 4DB, 5DB and 6DB are shown in Fig. 17. The ionization energy (I), electron affinity (A), Global hardness (η), chemical potential (μ) [48] and global electrophilicity power (ω) [49] of the three compounds are calculated using the HOMO and LUMO orbital energies by the relations discussed in section 3 and they are presented in Table 5. The energy value of frontier molecular orbital gap is determined as 3.7119, 3.5541 and 3.6343 eV for 4DB, 5DB and 6DB molecules, respectively. The calculated frontier molecular orbital gap is small; the chemical potential value of the molecules is greater and negative which demonstrates that the three molecules are polarizable and stable. On comparing the three compounds, it can be observed that the calculated HOMO-LUMO energy gap [50] is high for 4DB and low for 5DB, i.e, 4DB is more stable and non-reactive than 5DB.

Global chemical reactivity descriptors of molecules such as electro-negativity (χ), chemical potential (μ), chemical hardness (η), softness (S) and electrophilicity index (ω) are computed from ionization potential (I) and electron affinity (A) values as presented in our earlier paper on bipyridines [10]. The values of these Global chemical reactivity descriptors of the molecules under investigation are tabulated in Table 5. These parameters are helpful for understanding the various aspects of pharmacological formulations including drug design and the possible eco toxicological characteristics of the drug molecules.

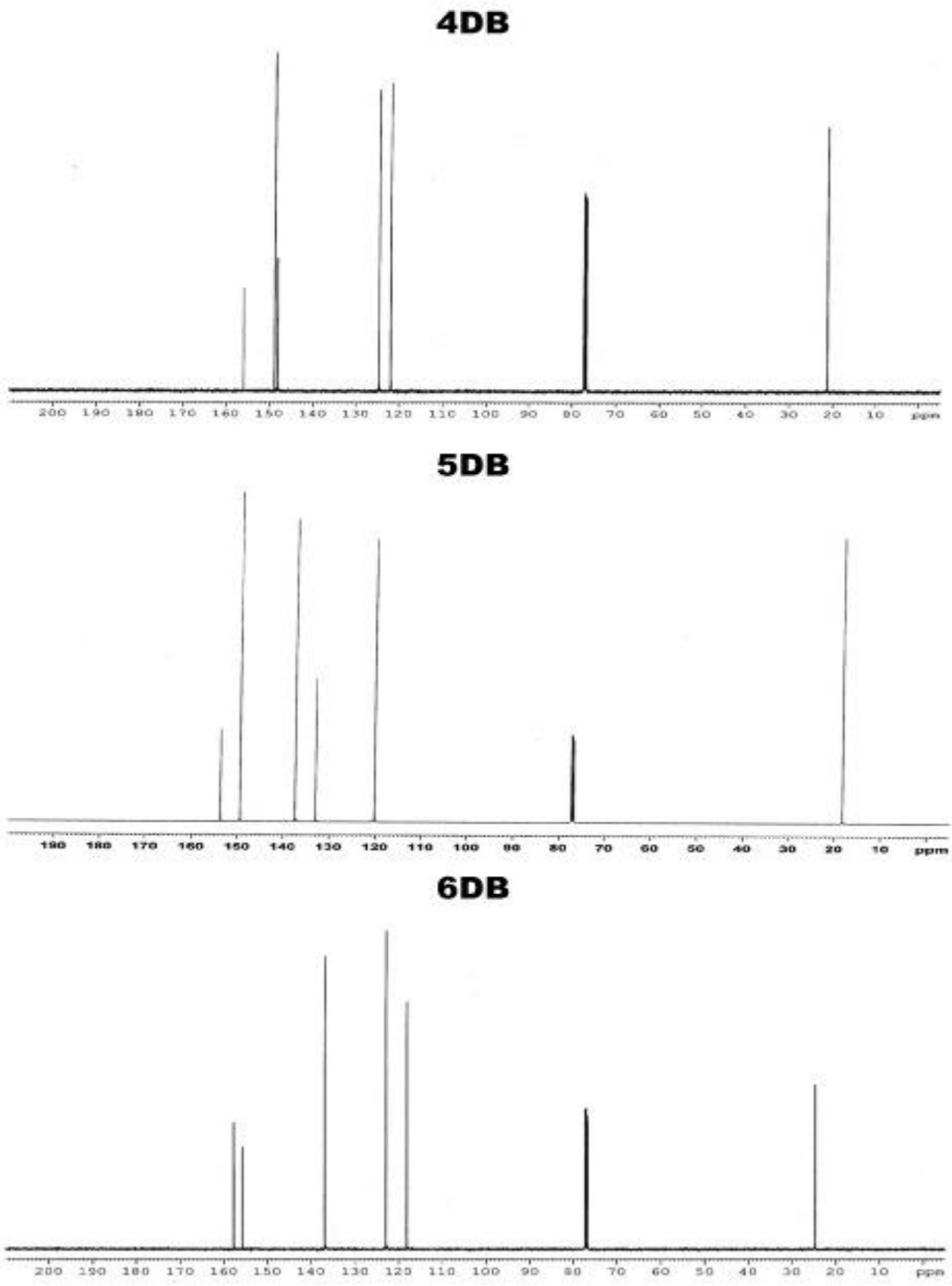

Fig. 14. Experimental ^{13}C NMR spectra of 4BD, 5DB and 6DB.

4.5. Analysis UV–Vis spectra

The wavelengths of absorption peaks in UV–Visible spectrum can be correlated with the types of bonds in a given molecule and are valuable in determining the functional groups within a molecule. The electronic absorption spectra of 4DB, 5DB and 6DB were computed with the help of calculations using TD-DFT/B3LYP/6-311++G(d,p) formalism. The observed and simulated UV–Vis spectra of the molecules 4DB, 5DB and 6DB are shown in Fig. 18 and spectral values are depicted in Table 6. The experimental UV–Vis spectra in solution show three absorption bands (λ_{max}) at 208.0, 239.8 and 280.4 nm in 4DB; 202.1, 243.4 and 288.0 nm in 5DB; and 205.1, 236.9 and 288.5 nm in 6DB. In simulated UV–Vis spectra of each of the three molecules, only one absorption band is seen, whereas the other two are not seen due to weak oscillator strengths. But, the computations yielded three absorption bands at 265, 280 and 292 nm for 4DB; 265, 288 and 289 nm for 5DB; and 270, 287 and 295 nm for 6DB which can be seen from Table 6. The absorption at 280.4, 288.0 and 288.5 nm, respectively in 4DB, 5DB and 6DB may be thought to occur due to n-π^* transition associated with nitrogen atoms of the pyridine rings and may be considered as dominant HOMO-LUMO excitation of the non-deprotonated contributions. The pair of absorptions at 239.8 and 208.0 nm; 243.4 and 202.1 nm; and 236.9 and 205.1 nm, respectively in 4DB, 5DB and 6DB may be ascribed to π-π^* transitions associated with carbons of pyridine rings. It can be seen from Table 6 that the computed

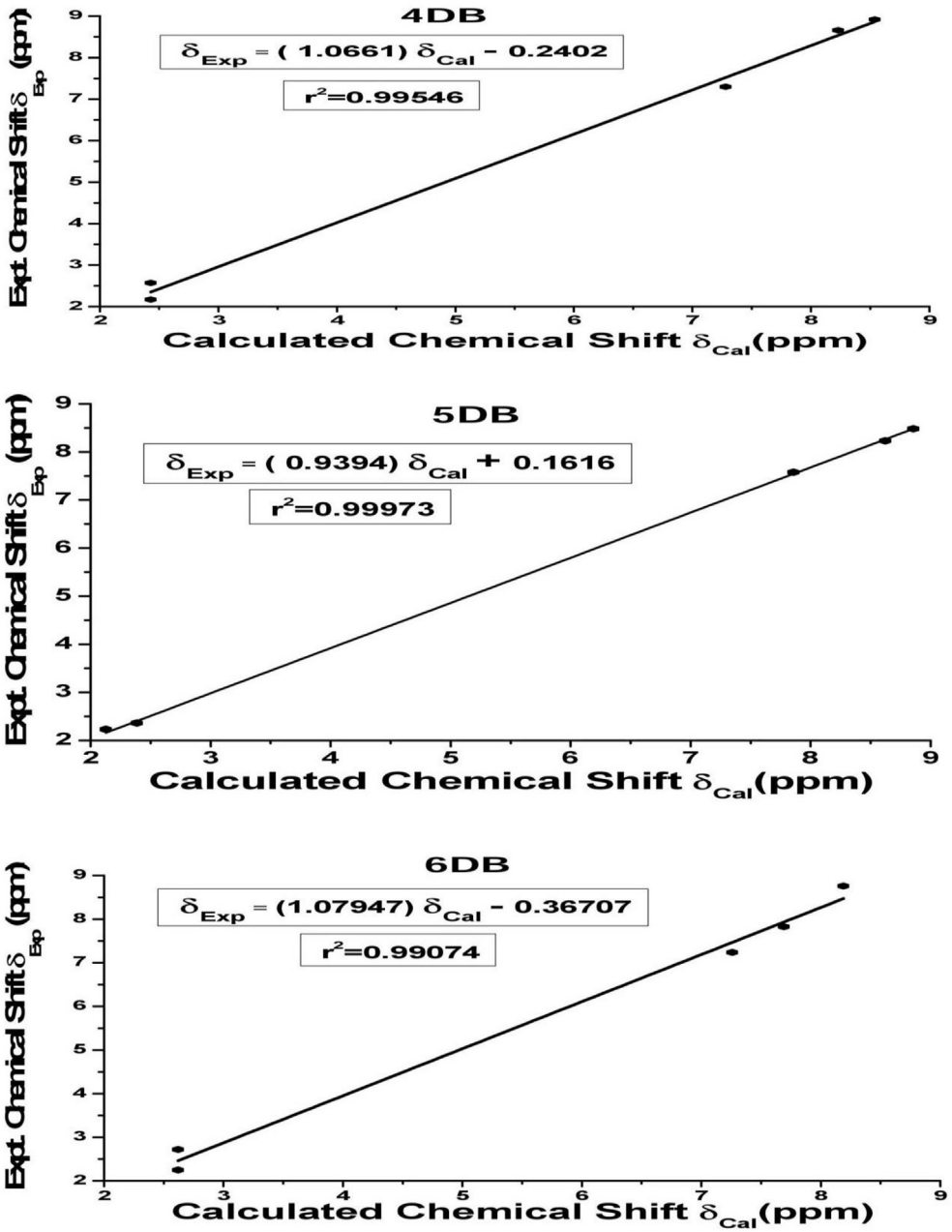

Fig. 15. Plot of experimental vs calculated ^{1}H NMR chemical shifts of 4DB, 5DB and 6DB.

absorptions agree reasonably well with the experimental absorptions for 4DB, 5DB and 6DB. The difference between the experimental and simulated frequencies may be due to the fact that the computations have been performed on a single molecule in the gaseous state, whereas the experimental values recorded in solid state in the presence of intermolecular interactions. The absorption band of 6DB fairly agrees with that proposed by Seyfi et al. [19] and Blanchet-Boiteux et al. [16].

4.6. Molecular electrostatic surface potential (MESP)

MESP at a point in the region around a molecule provides an indication of the net electrostatic effect formed at that point by the total charge distribution (electron + nuclei) of the molecule and correlates with dipole moments, electro-negativity, partial charges and chemical reactivity of the molecules. It is determined by mapping of molecular electrostatic potential (MEP) V(ř) onto the iso-electron density surface. The MEP, at any given point ř(x, y, z) is the sum of two opposing interaction energies (positive and negative). The positive interaction energy takes place from the interaction of nuclei of the molecule with a positive test charge (a proton) located at ř, whereas the negative interaction energy originates from the interaction of electrons of the molecule with the same test charge at ř [49,51]. MESP provides a visual method to understand the relative polarity and the regions of varying electron density of the molecule are indicated using the Colour grading [52]. The colour scheme for MESP is: red for electron rich (partial negative charge), blue for electron deficient (partial positive

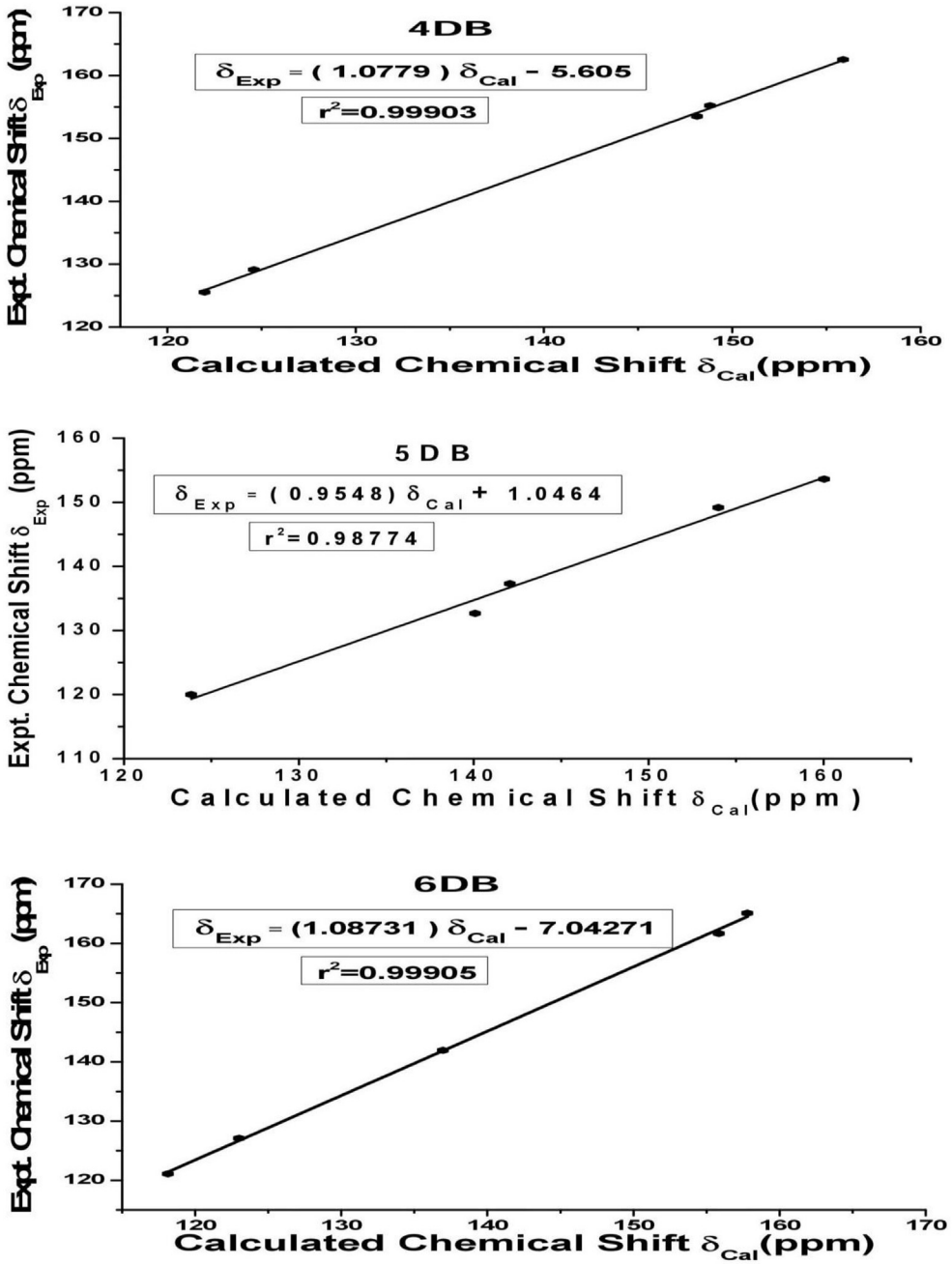

Fig. 16. Plot of experimental vs calculated ^{13}C NMR chemical shifts of 4DB, 5DB and 6DB.

charge), light blue (orange) for slightly electron deficient region, yellow for slightly electron rich region and green for neutral region. A visual demonstration of the chemically active sites and comparative reactivity of atoms in 4DB, 5DB and 6DB is shown in Fig. 19. As can be seen from the MESP map of these molecules, the regions having the negative potential are over the electronegative nitrogen atom of the pyridine ring, while the regions having the positive potential are over the hydrogen atom of methyl groups. The dominance of red colour at nitrogens of aromatic rings indicates the high electron rich region, whereas, yellow colour at carbons of aromatic rings indicates the slightly electron rich region.

4.7. Natural population analysis (NPA)

The computation of atomic charges plays a vital role in employing quantum mechanical calculations to molecular systems [53]. The natural charges affect the NLO property, electronic structure and vibrational properties of a molecule. The distribution of these charges in the neighborhood of the atoms indicates the formation of donor and acceptor pairs involving the charge transfer in the molecule [54]. The natural charges of 4DB, 5DB and 6DB evaluated by Natural Bond Orbital (NBO) analysis using DFT/B3LYP/6-311++G(d,p) level of theory are depicted in Table 7. The electronegative N2, C4, C6, N8, C10, C12, C13 and C14 atoms of 4DB

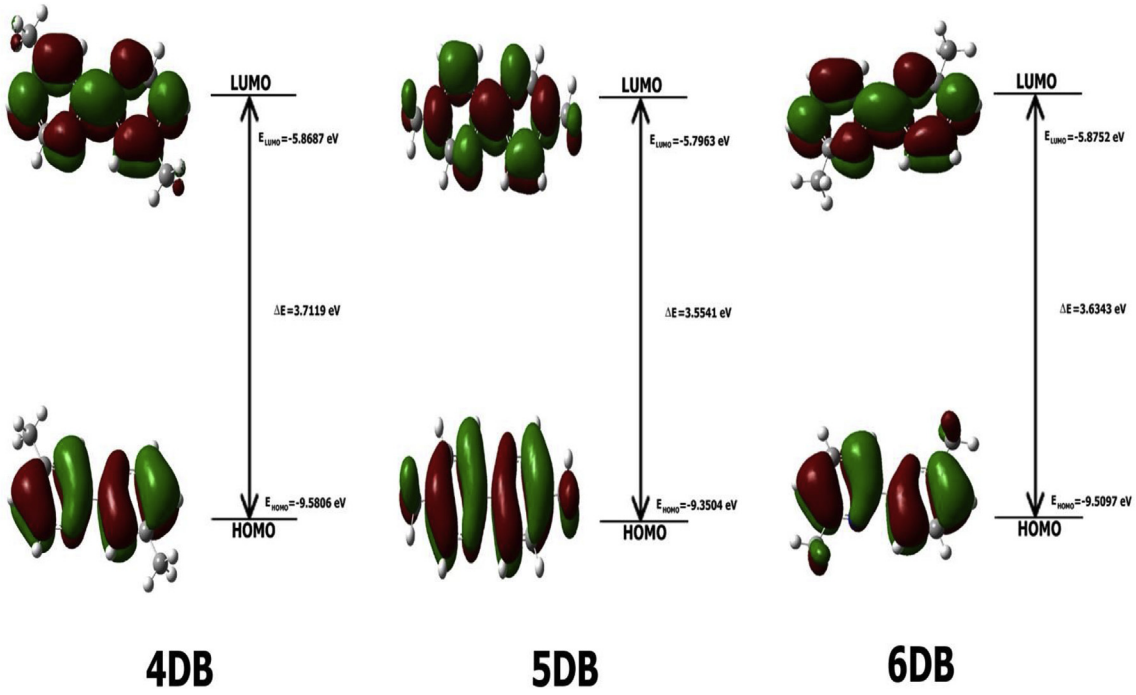

Fig. 17. Frontier molecular orbitals of 4DB, 5DB and 6DB.

Table 5
Frontier molecular orbital parameters of 4DB, 5DB and 6DB by DFT/B3LYP/6-311++G(d,p) method.

Frontier molecular orbital parameter	Value (in eV)		
	4DB	5DB	6DB
HOMO energy	−9.5806	−9.3504	−9.5097
LUMO energy	−5.8687	−5.7963	−5.8752
Frontier molecular orbital energy gap	3.7119	3.5541	3.6343
Ionization energy (I)	9.5806	9.3504	9.5096
Electron affinity (A)	5.8687	5.7963	5.8752
Global hardness (η)	1.8559	1.7770	1.8172
Global softness (S)	0.2694	0.2814	0.2751
Chemical potential (μ)	−7.7246	−7.5733	−7.6924
Electronegativity (χ)	7.7246	7.5733	7.6924
Global electrophilicity power (ω)	16.0753	16.1379	16.2815

compound, whereas N2, C4, C5, C6, N8, C10, C11, C12, C13 and C14 atoms of 5DB and 6DB molecules have negative charge values. The remaining electronegative atoms of the three molecules have positive charge values. The calculated natural positive and negative charge values of the three molecules can be seen from Table 7. Natural population analysis is a good way to account for differences in electronegativities of atoms within the molecule and frequently uses for supporting the MESP analysis. The results are in good agreement with those of MESP. MESP and NPA can be used for explaining and envisaging the reactive behaviour of various types of chemical systems in both electrophilic and nucleophilic reactions [55].

4.8. Thermodynamic parameters and rotational constants

Several calculated thermodynamic parameters and rotational constants for 4DB, 5DB and 6DB are presented in Table 8. The standard thermodynamic functions such as SCF energy, specific heat capacity at constant volume (C_v), entropy (S), vibrational energy (E_{vib}), zero-point energy (E_0) and rotational constants (A, B and C) are determined using rigid rotor harmonic oscillator approximation employing standard expressions [56–58] and with DFT employing B3LYP/6-311++G(d,p) level of theory. In the present DFT computations, these rotational constants A, B and C are calculated as 1755, 381 and 141 MHz for 4DB; 2867, 314 and 284 MHz for 5DB; and 1660, 400 and 323 MHz for 6DB, respectively. Here, all the mentioned thermodynamic calculations were done in gas phase and pertain to 1 mol of perfect gas at one atm. As per the second law of thermodynamics in thermo chemical field [59], the calculations can be used to compute the other thermodynamic energies and help to estimate the directions of chemical reactions.

5. Conclusions

The following inferences are made on the basis of investigation reported above.

(i) DFT calculations made for dimers of 4DB, 5DB and 6DB substantiate the existence of hydrogen bond. It is predicted that the hydrogen bond is strong in 4DB dimer and those formed in 5DB and 6DB dimmers are due to weak Van der Waals interactions.
(ii) 4DB, 5DB and 6DB molecules are found to have planar structure attaining lowest energy with C_1 point group symmetry.
(iii) Theoretically evaluated structure parameters for 4DB, 5DB and 6DB agree well with their experimental counterparts.
(iv) Plotted linear regression curves between experimental and calculated frequencies; and computed regression coefficient (0.99) show that they are in good agreement in three molecules. Further, measured IR and Raman spectra agree fairly well with their calculated spectra for 4DB, 5DB and 6DB.

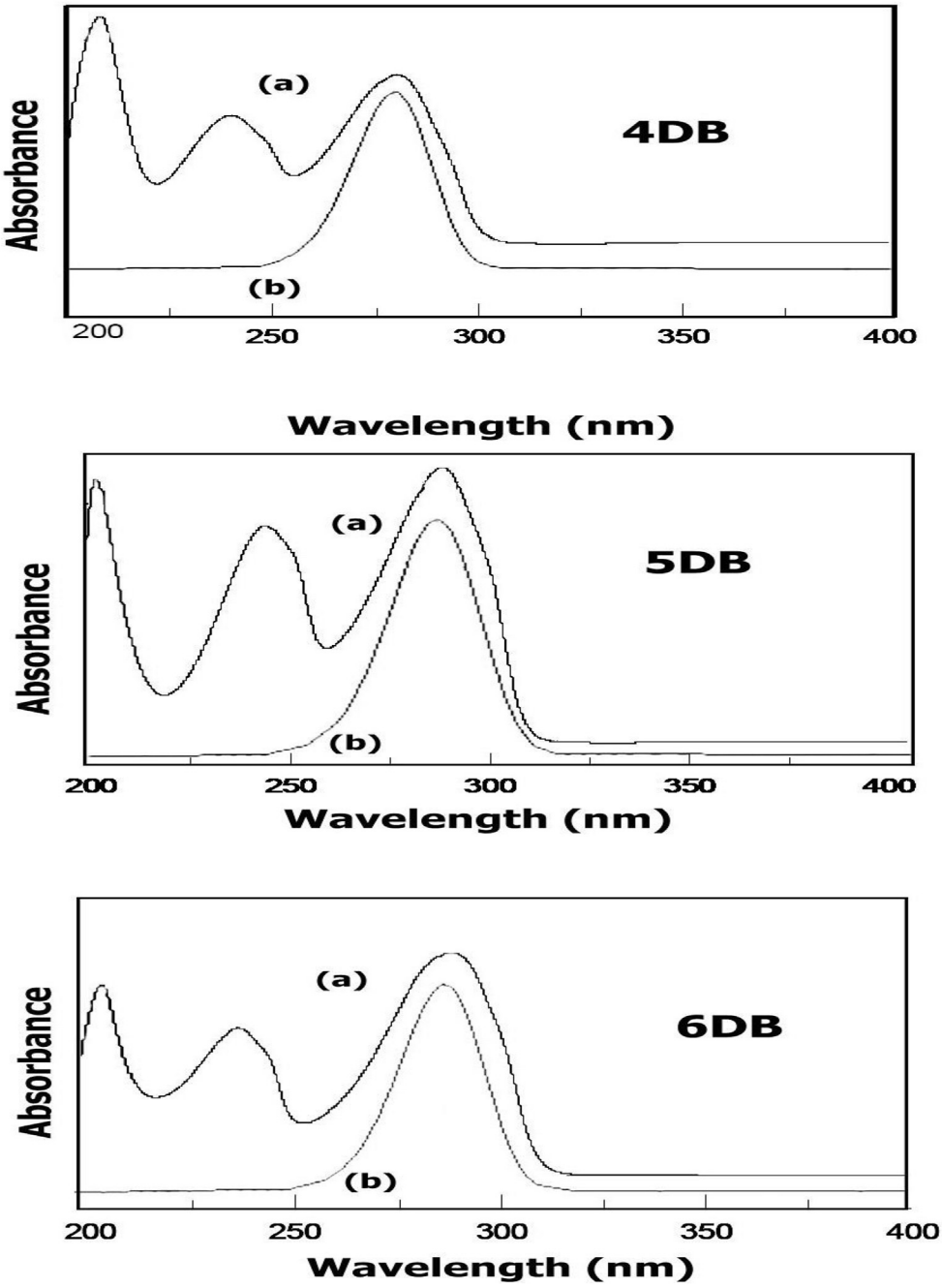

Fig. 18. UV−Vis Spectrum of 4DB, 5DB and 6DB (a) Experimental and(b) Simulated with DFT/B3LYP/6-311++G(d,p) formalism.

Table 6
Experimental and theoretical electronic absorption spectral values of 4DB, 5DB and 6DB.

Excited state	Wavelength λ (nm)						Excitation energies(eV)			Oscillator strengths (f)		
	Experimental			Theoretical								
	4DB	5DB	6DB	4DB	5DB	6DB	4DB	5DB	6DB	4DB	5DB	6DB
S1	208.0	202.1	205.1	265	265	270	4.678	4.678	4.592	0.0000	0.0000	0.0000
S2	239.8	243.4	236.9	280	288	287	4.428	4.305	4.320	0.6184	0.7713	0.5484
S3	280.4	288.0	288.5	292	289	295	4.246	4.290	4.202	0.0022	0.0032	0.0022

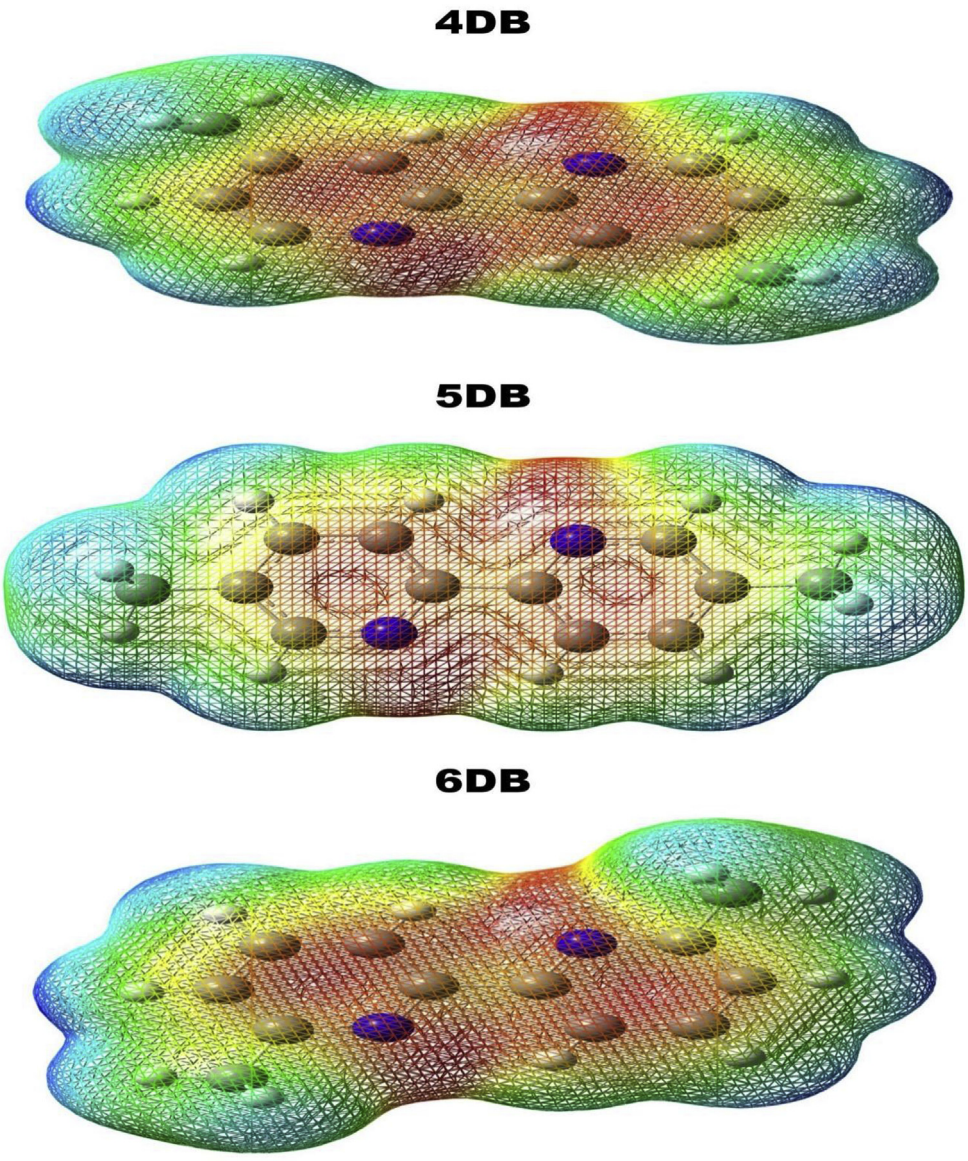

Fig. 19. Total electron density mapped with electrostatic potential surface of 4DB, 5DB and 6DB.

(v) Vibrational assignments of all the fundamental modes of 4DB, 5DB and 6DB are suggested unambiguously for the first time using PED.

(vi) Experimental chemical shifts, both δ_H and δ_C, correlate well with their theoretical counterparts as evidenced from linear regression plots.

(vii) The observed and simulated UV–Vis spectra of the molecules under investigation demonstrate that a strong absorption band occurs due to n-π^* transition associated with nitrogen atoms of the pyridine rings and two absorptions are obtained due to π-π^* transitions associated with carbons of pyridine rings.

(viii) The calculated HOMO and LUMO energies show that the charge transfer occurs from the donor atoms to the acceptor atoms through π-conjugated path within each of the three molecules. The large value of HOMO-LUMO energy gap and large negative chemical potential obtained in this study indicate that the chosen molecules are stable and unreactive.

(ix) The MESP map of these molecules shows that the negative potentials are over the electronegative nitrogen atom of the pyridine ring, whereas the positive potentials are over the hydrogen atom of methyl group. MESP map is quantified with the natural charges obtained by NBO analysis.

Table 7
Natural charge analysis of 4DB, 5DB and 6DB.

Atom	NBO (NPA) charges (in eV)		
	4DB	5DB	6DB
C1	0.18063	0.18500	0.19691
N2	−0.47234	−0.46295	−0.48517
C3	0.06532	0.05944	0.22346
C4	−0.24406	−0.06594	−0.24276
C5	0.00983	−0.16312	−0.16359
C6	−0.21410	−0.20806	−0.21014
C7	0.19981	0.16618	0.17758
N8	−0.47482	−0.46045	−0.48360
C9	0.06504	0.05987	0.22466
C10	−0.24415	−0.06575	−0.24279
C11	0.00987	−0.16333	−0.16323
C12	−0.22087	−0.20193	−0.20737
C13	−0.59383	−0.59049	−0.59737
C14	−0.59379	−0.59062	−0.59725
H1	0.18325	0.18034	0.20735
H2	0.20669	0.20287	0.20555
H3	0.23327	0.23481	0.23487
H4	0.18326	0.18035	0.20741
H5	0.20667	0.20288	0.20560
H6	0.23344	0.23469	0.23492
H11	0.21497	0.21252	0.21880
H12	0.21051	0.20805	0.21880
H13	0.21499	0.21252	0.19993
H21	0.21478	0.21252	0.21885
H22	0.21051	0.20807	0.20000
H23	0.21514	0.21252	0.21884

Table 8
Thermodynamic parameters (for 1 mol of perfect gas at one atm.) and rotational constants of 4DB, 5DB and 6DB.

Thermodynamic parameters	Value		
	4DB	5DB	6DB
SCF Energy (in 10^3 kJ mol^{-1})	−1507.483	−1507.479	−1507.492
Total energy (thermal), E_{total} (kcal mol^{-1})	140.566	140.549	140.430
Heat capacity at const. volume, C_V (cal $mol^{-1}K^{-1}$)	46.669	46.675	46.791
Heat capacity at const. presure, C_P (cal $mol^{-1}K^{-1}$)	48.655	48.661	48.777
Entropy, S (cal $mol^{-1}K^{-1}$)	114.728	111.785	111.958
Vibrational energy, E_{vib} (kcal mol^{-1})	138.788	138.772	138.653
Zero-point vibrational energy, E_0 (kcal mol^{-1})	132.738	132.801	132.689
Rotational constants (GHz)			
A	1.755	2.867	1.660
B	0.381	0.314	0.400
C	0.141	0.284	0.323

Acknowledgements

The authors sincerely acknowledge financial support, under SAP-DRS-II, extended by the University Grants Commission, New Delhi, India through their Lr.No.F.530/24/DRS-II, 2015 (SAP). They are thankful to Sophisticated Analytical Instrumentation Facility (SAIF), IIT Madras, Chennai, India, for spectral measurements (IR & Raman). They are also grateful to NIPER, Hyderabad for recording ^1H and ^{13}C NMR spectra and UV−Visible spectra.

Appendix A. Supplementary data

Supplementary data to this article can be found online at https://doi.org/10.1016/j.molstruc.2019.127089.

References

[1] N.R. Kelly, S. Goetz, Ch S. Haves, P.E. Kruger, Inorg. Chim. Acta 403 (2013) 102−109.
[2] A.E. Ozel, S. Kecel, S. Akyuz, J. Mol. Struct. 834 (2007) 548−554.
[3] N. Tadayon Por, A. Khaleghi, M. Yousefi, V. Amani, Inorg, Met,-Org, Nano-Metal Chem. 45 (2015) 1427−1433.
[4] L.F. Eckhard, N.G. Keats, L.A.Z. Summers, Naturforscher B33 (1978) 80−83.
[5] L.A. Summers, The Bipyridinium Herbicides, Academic Press, London, 1981.
[6] H.G. Grant, L.A.Z. Summers, Naturforscher B33 (1978) 118−119.
[7] S.H. Etaiw, M.M. El-bendary, Inorg. Chim. Acta 435 (2015) 167−173.
[8] F. Havas, N. Leygue, M. Danel, B. Mestre, Ch Galaup, C. Picard, Tetrahedron 65 (36) (2009) 7673−7686.
[9] T. Cassol, F.W. Joachim Demnitz, M. Navarro, E.A.D. Neves, Tetrahedron Lett. 41 (43) (2000) 8203−8206.
[10] J. Prashanth, B. Venkatram Reddy, G. Ramana Rao, J. Mol. Struct. 1117 (2016) 79−104.
[11] J. Prashanth, K. Ramaiah, B. Venkatram Reddy, Molecular Simulation /J. Experimental nanoscience, https://doi.org/10.1080/08927022.2019.1634807.
[12] M.A.V. Ribeiro da Silva, M.A.R. Matos, C.M.A. do Rio, V.M.F. Morais, J. Chem. Soc., Faraday Trans. 93 (17) (1997) 3061−3065.
[13] Kai-Long Zhong, Acta Crystallogr. C69 (2013) 1537−1540.
[14] Z. Khoshtarkib, A. Ebadi, R. Ahmadi, R. Alizadeh, Acta Crystallogr. E65 (2009), 01586.
[15] A. Sengul, M.B. Hursthouse, S.J. Coles, R.D. Gillard, Acta Crystallogr. C54 (1998) 661−662.
[16] C. Blanchet-Boiteux, P. Friant-Michel, A. Marsura, Jean-Bernard Regnouf-de-vains, M.F. Ruiz-Lopez, J. Mol. Struct. Theochem 811 (2007) 169−174.
[17] G. Bator, W. Sawka-Dobrowolska, L. Sobczyk, E. Grech, J. Nowicka-Scheibe, A. Pawlukojc, J. Wuttke, J. Baran, M. Owczarek, J. Chem. Phys. 135 (2011), 044509.
[18] Benjamin J. Pages, Y. Zhang, F. Li, J. Sakoff, J. Gilbert, J.R. Aldrich-Wright, Eur. J. Inorg. Chem. (2015) 4167−4175.
[19] S. Seyfi, R. Alizadeh, M. Darvish Ganji, V. Amani, Vacuum 139 (2017) 9−22.
[20] Li Ying-Ying, Ning ren, ShuMei He, Shi-Ping Wang, Jiang-Jun Zhang, J. Chem. Thermodyn. 135 (2019) 1−8.
[21] M.J. Frisch, et al., Gaussian 09, Revision B.01, Gaussian, Inc., Wallingford CT, 2010.
[22] A.D. Becke, J. Chem. Phys. 98 (1993) 5648−5652.
[23] C. Lee, W. Yang, R.G. Parr, Phys. Rev. B 37 (1988) 785−789.
[24] G. Fogarasi, X. Zhou, P.W. Tayler, P. Pulay, J. Am. Chem. Soc. 114 (1992) 8191−8201.
[25] T. Sundius, J. Mol. Struct. 218 (1990) 321−326.
[26] T. Sundius, Vib. Spectrosc. 29 (2002) 89−95.
[27] P. Pulay, G. Fogarasi, G. Pongor, J.E. Boggs, A. Vargha, J. Am. Chem. Soc. 105 (1983) 7037−7047.
[28] J.F. Arenas, I.L. Tocoón, J.C. Otero, J.I. Marcos, J. Mol. Struct. 476 (1999) 139−150.
[29] Z. Latajka, W.B. Person, K. Morokuma, J. Mol. Struct. Theochem. 135 (1986) 253−266.
[30] G. Kereztury, S. Holly, G. Besenyei, J. Varga, A. Wang, J.R. Durig, Spectrochim. Acta 49 (1993) 2007−2026.
[31] G. Kereztury, J. M Chalmers, in: P. R Griffith (Ed.) Vol. 1, John Wiley and sons Ltd., New York, 2002, pp. 71−87.
[32] K. Wolinski, R. Haacke, J.F. Hinton, P. Pulay, J. Comput. Chem. 18 (1997) 816−825.
[33] G. Scalmani, M.J. Frisch, J. Chem. Phys. 132 (2010) 1−15.
[34] A.D. Buckingham, Adv. Chem. Phys. 12 (1967) 107−142.
[35] G. Gece, Corros. Sci. 50 (2008) 2981−2992.
[36] K. Fukui, Science 218 (1982) 747−754.
[37] T.A. Koopmans, Physica 1 (1933) 104−113.
[38] T. Steiner, C−H···O hydrogen bonding in crystals, Crystallogr. Rev. 9 (2003) 177−228.
[39] T. Steiner, G.R. Desiraju, Distinction between the weak hydrogen bond and the Van Der Waals interaction, Chem. Commun. (1998) 891−892.
[40] G.R. Desiraju, C−H…O and other weak hydrogen bonds.From crystal engineering to v virtual screening, Chem. Commun. (2005) 2995−3001.
[41] F Biegler-kö nig, Jens schö nbohm, Update of the AIM2000-program for atoms in M molecules, J. Comput. Chem. 23 (2002) 1489−1494.
[42] E.B. Wilson Jr., J. Chem. Phys. 7 (1939) 1047−1052, 9 (1941) 76-84.
[43] E.B. Wilson Jr., Phys. Rev. 45 (1934) 706−714.
[44] G. Varsanyi, Assignments for Vibrational Spectra of Seven Hundred Benzene Derivatives, vol. 1, Adam Hilger, London, 1974.
[45] Jai Kishan Ojha, B. Venkatram Reddy, G. Ramana Rao, Spectrochim. Acta, Part A 96 (2012) 632−643.
[46] V. Arjunan, P. Ravindran, T. Rani, S. Mohan, J. Mol. Struct. 988 (2011) 91.
[47] N. Sinha, O. Prasad, V. Naryan, S.R. Shukla, Raman, J. Mol. Simul. 37 (2011) 153−163.
[48] N. Ozdemir, B. Eren, M. Dincer, V. Bekdemir, Mol. Phys. 108 (2010) 13−24.
[49] R.J. Parr, L.V. Szentp_aly, S. Liu, J. Am. Chem. Soc. 121 (1999) 1922−1924.
[50] D. Kivelson, R.R. Neiman, J. Chem. Phys. 35 (1961) 149−155.
[51] P. Politzer, J.S. Murray, Theor. Chem. Acc. 108 (2002) 134−142.
[52] C. Parlak, M. Akdogan, G. Yildirim, N. Karagoz, E. Budak, C. Terzioglu, Spectrochim. Acta A79 (2011) 263−271.

[53] S. Gunasekaran, S. Kumaresan, R. Arunbalaji, G. Anand, S. Srinivasan, J. Chem.Sci 120 (2008) 315.
[54] R. John Xavier, E. Gobinath, Spectrochim. Acta 97 (2012) 215–222.
[55] Z. Demircioglu, C.A. Kastas, B. Orhan, J. Mol. Struct. 1091 (2015) 183–195.
[56] G. Herzberg, Infrared and Raman Spectra of Polyatomic Molecules, D. Van Nostrand, New York, 1945.
[57] Kenneth S. Pitzer, William D. Gwinn, Mol. Struct. and Stat. Thermodynamics (1993) 33–46.
[58] Mohammad M. Ghahremanpour, Paul J. van Maaren, Jonas C. Ditz, Roland Lindh, David van der Spoel, J. Chem. Phys. 145 (2016).
[59] V. Balachandran, V. Karunakaran, Spectrochim. Acta, Part A 106 (2013) 284–298.